INTERNAL RESONANCE RAMAN SCATTERING OF CHARACTERISTIC TARGET K X RAYS IN THICK SILICON TARGETS

by

JAMES M. HALL

B.S., Southern Colorado State College, 1974

A MASTER'S THESIS

submitted in partial fulfillment of the

requirements for the degree

MASTER OF SCIENCE

Department of Physics

KANSAS STATE UNIVERSITY
Manhattan, Kansas

1977

Approved:

Patrick Richard
Major Professor

I hear and I forget . . . I do and I understand.

Chinese Proverb

TABLE OF CONTENTS

LIST OF TABLES

LIST OF FIGURES

ACKNOWLEDGMENTS

I would like to thank my wife, Kathy, for her love, patience, and support and for keeping her head while I was losing mine.

I would like to thank my parents for their love and encouragement.

I wish to thank Keith Jamison for his help and encouragement during the course of this experiment and Carl Schmiedekamp for his many helpful comments and suggestions during the writing of this thesis.

I am deeply indebted to Larry Weaver, James McGuire, and Pat Richard for their help in guiding me through some of the more detailed calculations involved in this work.

I would like to thank Dea Richard for her expert typing of difficult material and for her patience in putting up with my numerous revisions.

I would also like to acknowledge the financial support of the U. S. Energy Research and Development Administration under Contract No. EY-76-S-02-2753.

James Hall
September 1977

INTRODUCTION AND EXPERIMENT

(a.) Introduction

In a recent study of the low energy satellite structure of silicon K x-ray spectra[1] a small discontinuity was observed between the $KL_{23}L_{23}$ radiative Auger structure (RAE) and the first radiative electron rearrangement (RER) peak. This structure has an energy equal to the $K\alpha_{1,2}$ x-ray energy minus the $L_{2,3}$ binding energy and its spectral shape resembles an inverted absorption edge. Figure 1 displays a Si K x-ray spectrum obtained for 1.5 MeV H^+ on a thick Si target. The small edge-shaped peak labled RS at $\sim$ 1640 eV is the structure of interest. Similar structures have been observed in photon induced Si x-ray spectra by Åberg et al.[2] and have been attributed to internal resonance Raman scattering (IRRS) of characteristic Kα x rays off of the K-shell of a neighboring Si atom.[3] In this process (Fig. 2) a Kα photon produced within a thick solid target by external photon or ion bombardment scatters off of a nearby ground state Si atom producing a virtual intermediate state with a K-shell hole. The K-shell hole is then filled in the transition to the final state by an L-shell electron emitting the outgoing photon, ω_f. Since the ejected (and now homeless) K electron must undergo a "virtual free" to "free" transition in going to the final state we must modify ω_f in order to allow for energy conservation. Equating the total energy (atom + photon field) of the initial and final states we obtain:

$$\hbar\omega_i = \hbar\omega_{K\alpha} = \hbar\omega_f + \hbar\omega_L + \epsilon_K$$

Figure 1 Low energy Si K x-ray spectra by Jamison et al.[1] showing the RAE, resonance Raman, and RER structures in relation to the normal Kα and first satellite lines.

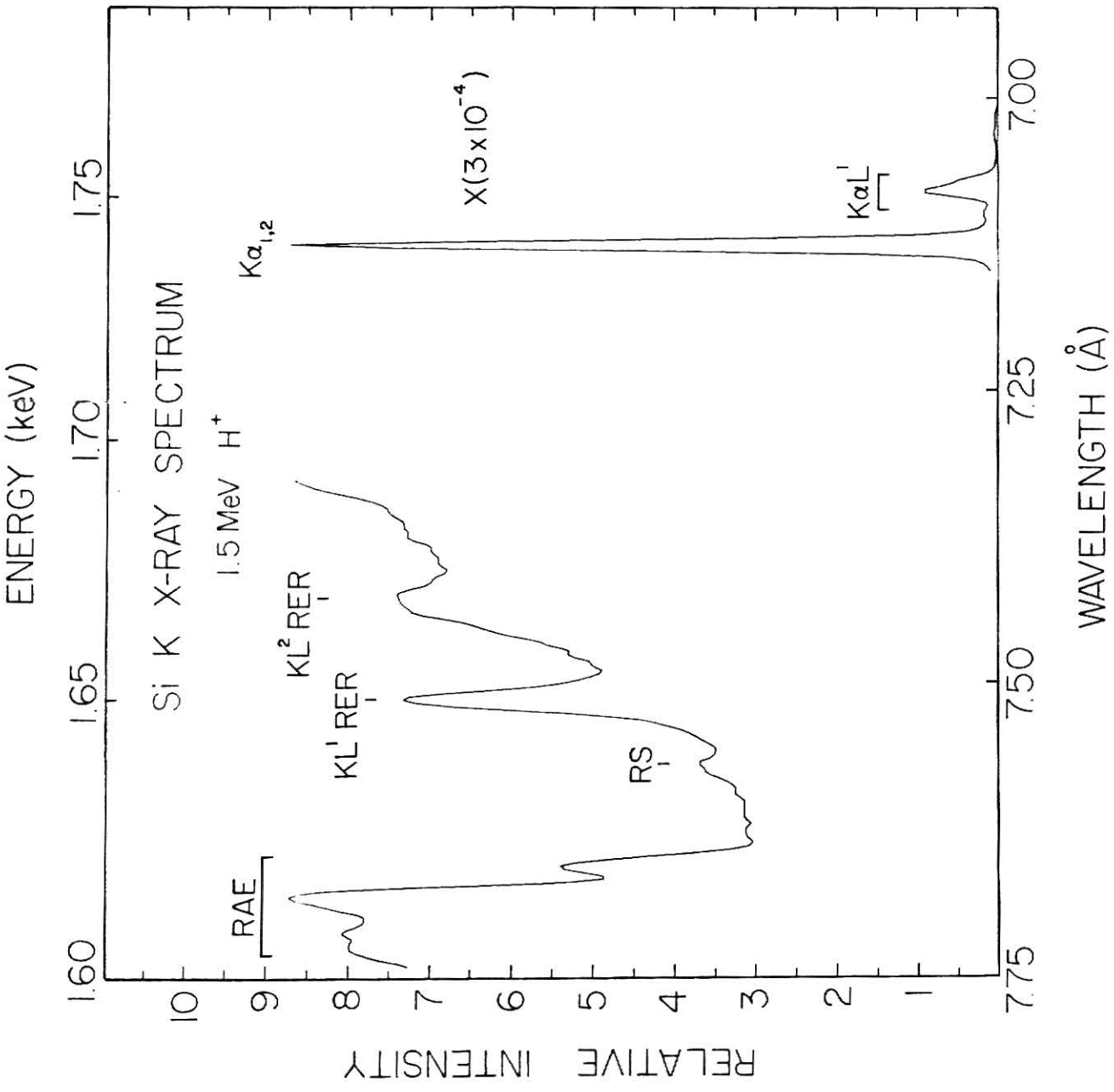
ENERGY (keV)
1.60
1.65
1.70
1.75
Si K X-RAY SPECTRUM
1.5 MeV H+
Kα1,2
X(3x10-4)
RAE
KL2RER
KL1RER
RS
KαL1
RELATIVE INTENSITY
10
9
8
7
6
5
4
3
2
1
7.75
7.50
7.25
7.00
WAVELENGTH (Å)

Figure 2 Schematic of the resonance Raman process.

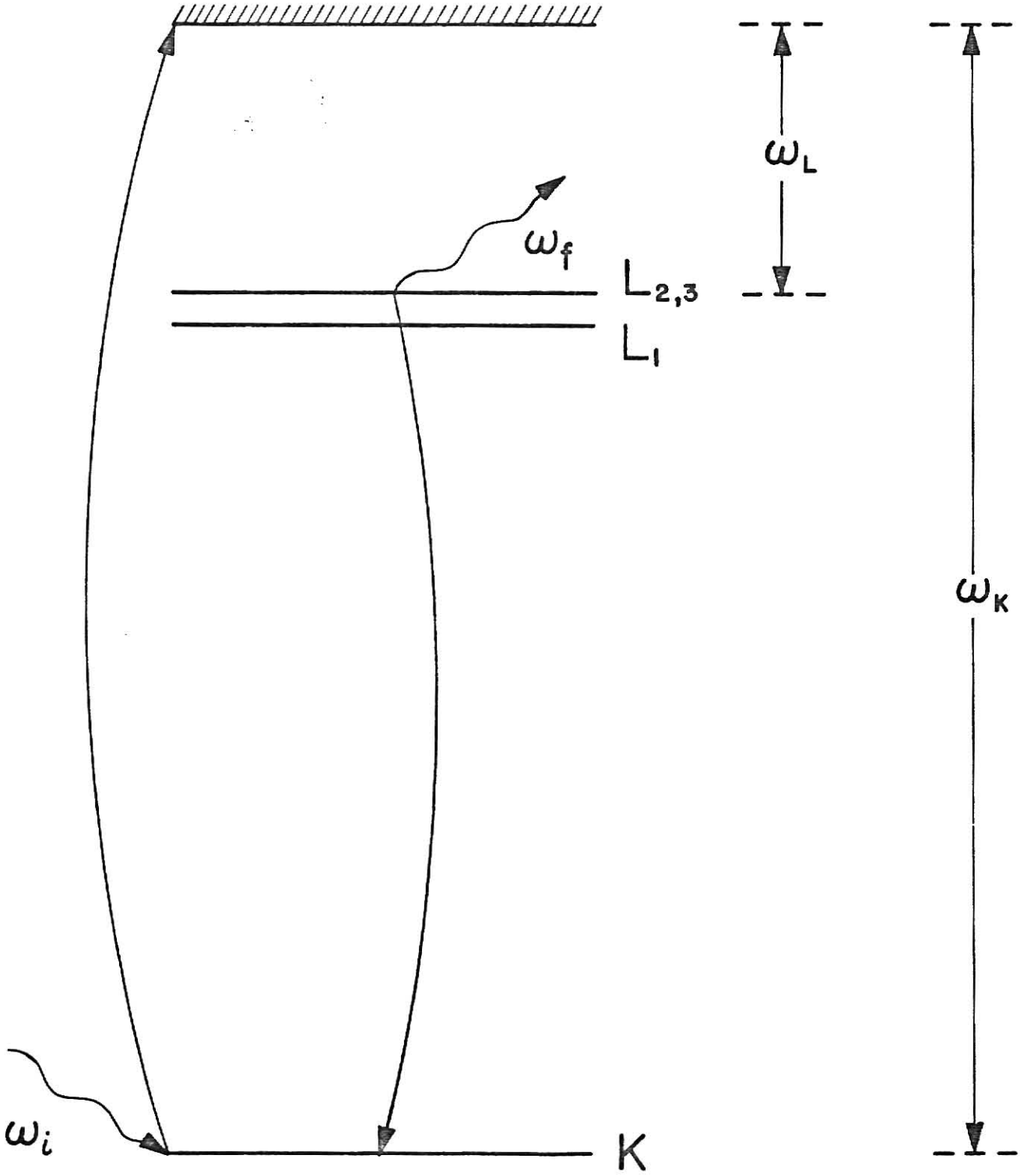
ω_L
ω_f
$L_{2,3}$
L_1
ω_K
ω_i
K

and thus:

$$\hbar\omega_f = \hbar\omega_{K\alpha} - \hbar\omega_L - \varepsilon_K \tag{1.1}$$

where $\hbar\omega_L$ represents the energy of an L-shell hole state and ε_K is the final energy of the ejected K electron. Since the ejected electron and scattered photon are free to share available energy within the bounds of Eqn. (1.1) we may rewrite Eqn. (1.1) as:

$$\hbar\omega_f \leq \hbar\omega_{K\alpha} - \hbar\omega_L \tag{1.2}$$

where the equality sign holds in the case for $\varepsilon_K = 0$. This then gives rise to an edge-shaped structure tailing off at low energies as observed. Note that the parameters associated with the IRRS process should be independent of the means of production (photon or ion) of the initial Kα photon.

The radiative Auger effect (RAE) was first observed in the K x-ray spectra of Mg, Al, Si, and S by Åberg and Utriainen[4] in 1969 and can roughly be described as a two-electron single-photon transition in which an outer-shell electron $n_f\ell_f$ jumps into a pre-existing inner-shell hole $n_i\ell_i$ (emitting the final photon ω_f) and another outer-shell electron $n_{f'}\ell_{f'}$ is excited to a bound or continuum state $\varepsilon\ell$. The photons emitted in a radiative Auger transition have both a discrete (when $\varepsilon\ell$ is a bound state) and continuous (when $\varepsilon\ell$ is a continuum state) distribution of energies given by:

$$\hbar\omega_f = I(n_i\ell_i) - I(n_f\ell_f) - I(n_f,\ell_f,)^* - \varepsilon_\ell \tag{1.3}$$

where the I's represent the appropriate ionization energies and, in particular, $I(n_f,\ell_f,)^*$ represents the $n_f,\ell_f,$ ionization energy in the presence of an $n_f\ell_f$ vacancy. Again the ejected electron and final photon may share the available energy within the bounds of Eqn. (1.3) and thus we obtain:

$$\hbar\omega_f \leq I(n_i\ell_i) - I(n_f\ell_f) - I(n_f,\ell_f,)^* \tag{1.4}$$

where the equality holds for $\varepsilon_\ell = 0$. Thus the RAE process also exhibits an edge-shaped structure tailing off at low energies (Fig. 1). In the case of a $KL_{23}L_{23}$ radiative Auger transition Eqns. (1.3) and (1.4) may be written as:

$$\begin{aligned}\hbar\omega_f &= I(1s) - I(2p) - I(2p)^* - \varepsilon_K \\ &= \hbar\omega_K - \hbar\omega_L^* - \varepsilon_K\end{aligned} \tag{1.5}$$

and

$$\begin{aligned}\hbar\omega_f &\leq I(1s) - I(2p) - I(2p)^* \\ &\leq \hbar\omega_{K\alpha} - \hbar\omega_L^*\end{aligned} \tag{1.6}$$

where we do not distinguish between the L_{II} and L_{III} subshells. Comparing Eqns. (1.1) and (1.5) we see that proper definition of the appropriate

$L_{2,3}$ ionization energy is an important consideration in separating the radiative Auger and resonance Raman effects experimentally. Direct observation of IRRS as a separate structure from the RAE then allows us to differentiate between scattering type processes which are internal to the atom (RAE) and those which are external to the atom (resonance Raman).

Radiative electron rearrangement (RER) is a third type of single-photon two-electron transition first described by Jamison et al.[5] in 1975. In this process a K x-ray is emitted coincident with two 2s electrons undergoing a rearrangement. One of the 2s electrons fills the K-shell vacancy while the other is promoted to the 2p subshell. This process thus requires that there be at least one 2p vacancy present in the atom in addition to the 1s vacancy. The lowest-energy RER is the transition from a state with one 1s and one 2p vacancy (KL^1 RER in Fig. 1). Since the addition of each L-shell vacancy increases the energy of the RER transition, an RER satellite sequence is expected and observed (Fig. 1).

The energy systematics of the RAE, IRRS, and RER are shown in Fig. 3. Silicon is seen to be the first element for which the IRRS process is easily observed in the region between the $KL_{23}L_{23}$ RAE edge and the first RER satellite. The sulfur IRRS point on Fig. 3 was taken from photon induced spectra by Åberg and Utriainen.[4] The IRRS process has also been observed in photon induced CaO and TiO_2 spectra by Sawada et al.[6] (not shown in Fig. 3).

Previous experimental work directed specifically at studying the resonance Raman process has taken two basic approaches. Sparks[7]

Figure 3 Energy systematics of the low energy Si K x-ray structure. Peak positions are plotted in terms of separation from the characteristic Kα line. Solid lines are theoretical separations based on Jamison et al.[1] (RER), Shirley[25] (RAE), and Eqn. (1.2) using x-ray energies from Bearden[26] (IRRS). Resonance Raman scattering of both Kα and $K\alpha L^1$ radiation is shown. Experimental points are from Jamison et al.[1] (RER,RAE), Åberg et al.[4] (S IRRS), and this work (Si IRRS).

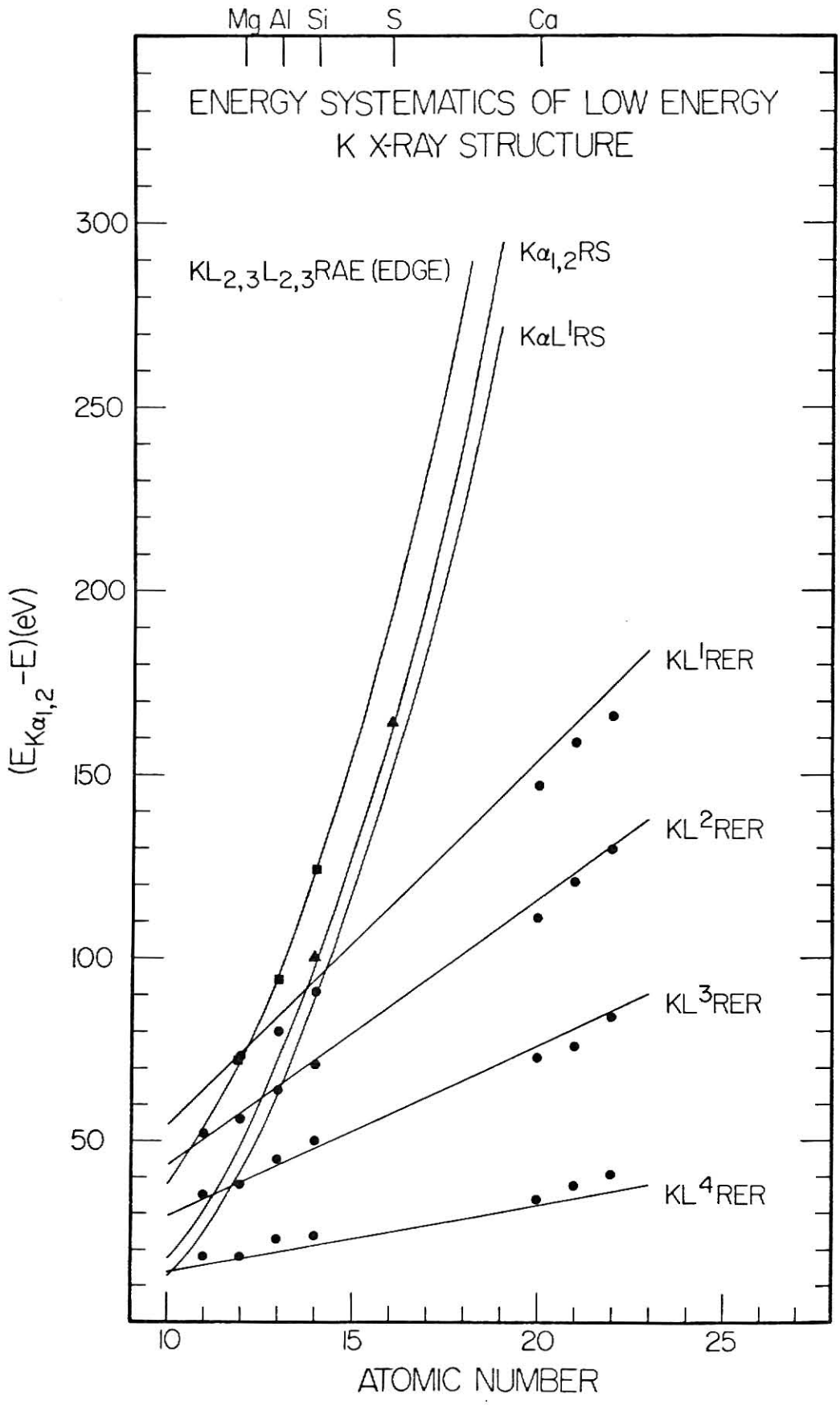
Mg Al Si S Ca
ENERGY SYSTEMATICS OF LOW ENERGY
K X-RAY STRUCTURE
KL2,3L2,3RAE (EDGE)
Kα1,2RS
KαL1RS
KL1RER
KL2RER
KL3RER
KL4RER
(EKα1,2 -E)(eV)
300
250
200
150
100
50
10
15
20
25
ATOMIC NUMBER

and Bannett et al.[8] have used monochromatic Cu Kα and Mo Kα x rays incident on Ni, Cu, Zn, Ge, and Ta targets to study the scattering cross section associated with the resonance Raman process while Eisenberger et al.[9] has used synchrotron radiation incident on Cu metal to investigate the energy systematics of the process over an energy range extending from the Cu K absorption edge to ∿ 500 eV below it. Theoretical calculations of the scattering cross section for Cu Kα radiation incident Ni, Cu, Zn, and Ge have been made by Bannett and Freund[10] and more recently by Tulkki and Åberg.[11] To this author's knowledge there has been no published work to date dealing specifically with the internal resonance Raman process described in this work.

The purpose of this thesis is to investigate the IRRS process in ion induced Si K x-ray spectra taken from thick targets and, if possible, to obtain an estimate for the scattering cross section. The following subsection will discuss the experimental procedure involved. In Section II of this thesis we will attempt to develop the theoretical scattering cross section for the resonance Raman process based on Fermi's Golden Rule taken to second order. Section III deals with the experimental extraction of an internal inelastic scattering cross section from thick target x-ray yields. Section IV contains an analysis of the data obtained in this experiment and a conclusion. There are two appendices. Appendix A outlines the development of Section III in the case of photon induced spectra. Appendix B gives a listing of the two computer codes used to extract the scattering cross section from thick target x-ray yields.

(b.) Experiment

The experiment consisted of bombarding a thick Si target with proton beams of 1.5 MeV and 2.0 MeV. A four-inch ARL curved crystal vacuum spectrometer was positioned at 90° with respect to the beam axis. The Si target was positioned at 45° with respect to both the beam and spectrometer axis. Spectra were taken with the spectrometer Rowland circle perpendicular to the beam axis ($\parallel$ mode) as well as coplanar with the beam axis ($\perp$ mode). In the $\parallel(\perp)$ mode the spectrometer is sensitive to that component of the emitted radiation which is polarized parallel (perpendicular) to the beam axis. The intensity of the first RER peak was observed to decrease in going from the $\parallel$ to $\perp$ mode due to polarization effects but no appreciable change in the Raman edge was noted. Most of the data were taken in the $\parallel$ mode. The beam current was integrated directly off of the thick target and at each angular setting of the crystal the x-ray intensity was accumulated for a preset number of microCoulombs of beam current. The spectrometer was fitted with 0.015 in. object (crystal) and image (proportional counter) slits. The detector used was a flow mode proportional counter fitted with a 2-μm Makrofol window. The counter used a P10 gas flow (10% methane; 90% argon) and was operated at a negative bias of 2150 V.

The proton beams were produced by the KSU single-stage AK-N Van de Graaff accelerator. The general layout of the accelerator and experiment station is shown in Fig. 4. Monoenergetic beams were momentum analyzed by a switching magnet and energy controlled by a fast-feedback slit control system. The beams were then focussed by an electrostatic quadrupole and collimated to a 2-mm spot before striking

Figure 4 Schematic of AK-N single-stage Van de Graaff accelerator and experiment station.

3MV VAN DE GRAAFF

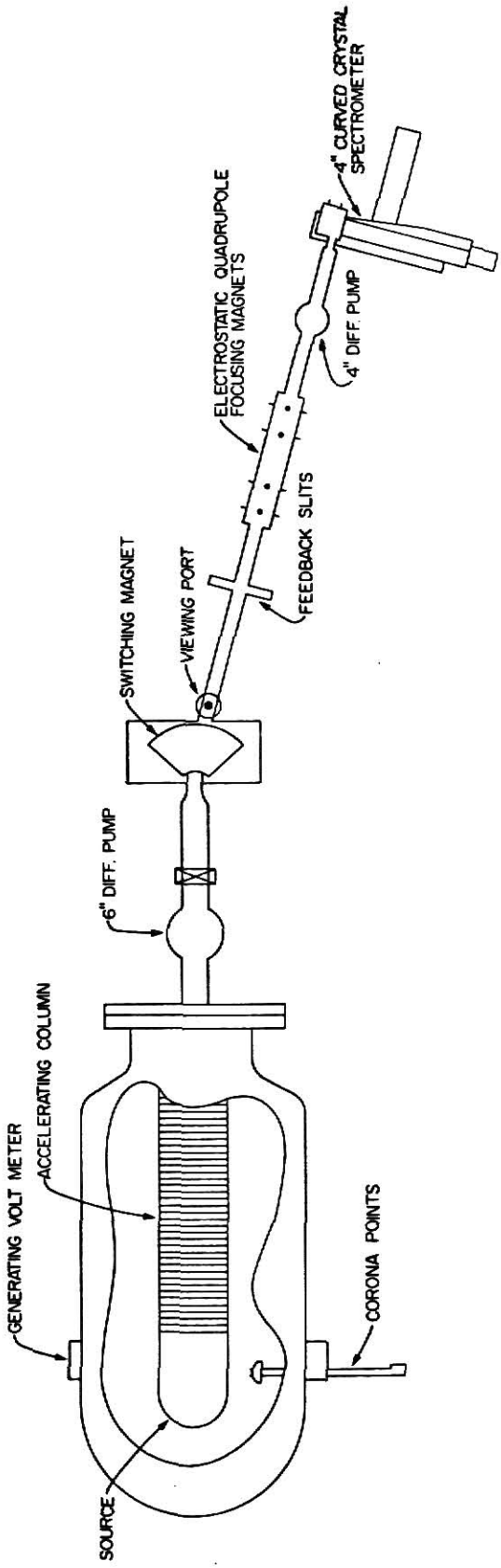

the target. Typical beam currents in the range of 3 to 6 μA were used to scan the x-ray region containing the RAE, IRRS, and RER processes. A reduced beam current of ∿ 150 nA was used to scan the x-ray region in the vicinity of the Kα peak and its first satellite in order to obtain the ratio $K\alpha L^{1}/K\alpha_{1,2}$. The reduced beam current was necessary in order to prevent pulse pileup and pulse-height defects in the proportional counter-preamplifier-amplifier system due to high count rates. The data were accumulated in a Nuclear Data 100 analyzer with a multiscaling device allowing for a variable spectrometer step size and variable integrated current per spectrometer step. The spectrometer step size used in this experiment was 0.00067 Å. The data were punched on paper tape for later off-line analysis on a PDP-15 computer.

In order to insure that the low-intensity Raman edge was not produced by geometrical effects due to the analyzing crystal used in the spectrometer, two different crystals were used to observe this effect. Si x-ray spectra obtained with ammonium dihydrogen phosphate (ADP) and ethylene diamine tartrate (EDdT) crystals seemed to give identical results although the ADP spectra were lower in overall intensity. Most of the spectra taken in this experiment were taken using the EDdT crystal due to its higher reflectivity in the energy range of interest (∿ 1600 to ∿ 1660 eV). All spectra were obtained in first order (i.e. $n\lambda = \lambda = 2d \sin\theta$ for Bragg's Law).

THEORETICAL DEVELOPMENT

In this section we will consider the scattering of light by an atom.[12,13] In general the scattering process consists of the absorption of a primary photon of energy $\hbar\omega_i$ by an atom in a state $|i\rangle$ followed by the emission of a secondary photon of energy $h\omega_f$ leaving the atom in some final state $|f\rangle$. When the initial and final states of the atom are the same ($|i\rangle = |f\rangle$; elastic) the frequency of the photon is not changed in the scattering process (in general only the direction of propagation is changed). This is called Rayleigh scattering. If the state of the atom changes during the scattering process ($|i\rangle \neq |f\rangle$; inelastic) then the energy of the scattered photon will, in general, differ from the energy of the incident photon. This sort of scattering process is called Compton or Raman scattering (it should be noted that in the x-ray region Raman scattering does not necessarily imply that the final state is a discrete state as is usually the case in the optical region.) Compton and Raman scattering differ essentially in the domains of the parameters $\hbar\omega_i/I$ and Kr where I is an inner-shell binding energy, r is a characteristic radius of the electron orbits, and K is a net momentum transfer. The scattering is called Compton scattering if $\hbar\omega_i >> I$ and $Kr >> 1$ (i.e. the electron is considered essentially free) and Raman scattering if $\hbar\omega_i \lesssim I$ and $Kr \lesssim 1$. In the case of Raman scattering of silicon Kα radiation off of the silicon K shell, we have $\hbar\omega_i = 1739$ eV $\lesssim 1839$ eV $= I_k$ and Kr (max) $\sim 0.03 \lesssim 1$ as required.

We will attempt to calculate the differential cross section for Raman scattering off of the K shell of an atom by direct evaluation using second order perturbation theory.

(a.) *The Hamiltonian*[12]

The classical Hamiltonian for a system of charged, spinless particles interacting with a radiation field in the non-relativistic approximation is given by:

$$H = H_R + \sum_j \frac{1}{2m_j} (\bar{p}_j - q_j \bar{A}(\bar{r}_j))^2 + \sum_{j \neq i} \sum_i \frac{1}{2} (q_i q_j / 4\pi\epsilon_o r_{ij}) \quad (2.1)$$

where H_R is the Hamiltonian for a free radiation field:

$$H_R = \sum_{\alpha=\{\bar{k},\lambda\}} a_\alpha^\dagger a_\alpha \hbar\omega_\alpha \quad (2.2)$$

with $\bar{k}$ being the photon wave vector and λ being its polarization index (1 or 2 in a linear polarization basis and + or - in a circular polarization basis). The summation extends over all photon modes $\{\bar{k},\lambda\}$ which exist in the field.

Equation (2.1) may be expanded into the following form:

$$H = H_R + \left\{ \sum_j p_j^2/2m_j + \sum_{j \neq i} \sum_i \frac{1}{2} (q_i q_j / 4\pi\epsilon_o r_{ij}) \right\}$$

$$- \sum_j (q_j/2m_j)(\bar{p}_j \cdot \bar{A}(\bar{r}_j) + \bar{A}(\bar{r}_j) \cdot \bar{p}_j) + \sum_j (q_j^2/2m_j) A^2(\bar{r}_j)$$

$$= H_R + \left\{ \sum_j p_j^2/2m_j + \sum_{j \neq i} \sum_i \frac{1}{2} (q_i q_j / 4\pi\epsilon_o r_{ij}) \right\}$$

$$- \sum_j (q_j/m_j) \bar{A}(\bar{r}_j) \cdot \bar{p}_j + \sum_j (q_j^2/2m_j) A^2(\bar{r}_j) \quad (2.3)$$

where we have used the commutation relation $[\bar{p},f(x)] = -ih\bar{\nabla}f(x)$ and the choice of the Coulomb gauge to require that $[\bar{p},\bar{A}(\bar{r})] = \bar{p}\cdot\bar{A}(\bar{r}) - \bar{A}(\bar{r})\cdot\bar{p} = -ih\bar{\nabla}\cdot\bar{A}(\bar{r}) = 0$. The total Hamiltonian for the system may now be written as the sum of three parts:

$$H = H_R + H_{ATOM} + H_{INT}$$

where

$$H_{ATOM} = \sum_j p_j^2/2m_j + \sum_{j\neq i}\sum_i \frac{1}{2}\,(q_i q_j/4\pi\epsilon_o r_{ij}) \quad ,$$

$$H_{INT} = -\sum_j (q_j/m_j)\bar{A}(\bar{r}_j)\cdot\bar{p}_j + \sum_j (q_j^2/2m_j)A^2(\bar{r}_j) \tag{2.4}$$

and H_R is given by Eqn. (2.2). The vector potential operator $\bar{A}(\bar{r}_j)$ is given by:

$$\bar{A}(\bar{r}_j) = \sum_\alpha (\hbar/2\epsilon_o\omega_\alpha L^3)\left\{a_\alpha \bar{e}_\alpha e^{i\bar{k}_\alpha\cdot\bar{r}_j} + a_\alpha^\dagger \bar{e}_\alpha^{\,*} e^{-i\bar{k}_\alpha\cdot\bar{r}_j}\right\} \tag{2.5}$$

where $\bar{e}_\alpha$ is a polarization basis vector. The electron-photon interaction Hamiltonian H_{INT} is the sum of two operators, H_1 and H_2, which may be given as:

$$H_1 = \frac{e}{m}\sum_\alpha (\hbar/2\epsilon_o\omega_\alpha L^3)^{1/2}\left\{a_\alpha \bar{e}_\alpha\cdot\sum_j \bar{p}_j\, e^{i\bar{k}_\alpha\cdot\bar{r}_j}\right.$$

$$\left. + a_\alpha^\dagger\, \bar{e}_\alpha^{\,*}\cdot\sum_j \bar{p}_j\, e^{-i\bar{k}_\alpha\cdot\bar{r}_j}\right\} \tag{2.6}$$

$$H_2 = \frac{e^2}{2m} \sum_{\alpha\alpha'} (\hbar/2\epsilon_o L^3)(1/\sqrt{\omega_\alpha \omega_{\alpha'}})$$

$$\times \sum_j \Big\{ (\bar{e}_\alpha \cdot \bar{e}_{\alpha'}) a_\alpha a_{\alpha'} \, e^{i(\bar{k}_\alpha + \bar{k}_{\alpha'})\cdot \bar{r}_j}$$

$$+ (\bar{e}_\alpha \cdot \bar{e}^*_{\alpha'}) a_\alpha a^\dagger_{\alpha'} \, e^{i(\bar{k}_\alpha - \bar{k}_{\alpha'})\cdot \bar{r}_j}$$

$$+ (\bar{e}^*_\alpha \cdot \bar{e}_{\alpha'}) a^\dagger_\alpha a_{\alpha'} \, e^{-i(\bar{k}_\alpha - \bar{k}_{\alpha'})\cdot \bar{r}_j}$$

$$+ (\bar{e}^*_\alpha \cdot \bar{e}^*_{\alpha'}) a^\dagger_\alpha a^\dagger_{\alpha'} \, e^{-i(\bar{k}_\alpha + \bar{k}_{\alpha'})\cdot \bar{r}_j} \Big\} \quad . \tag{2.7}$$

The operator $H_{INT} = H_1 + H_2$ will be treated as a perturbation while $H_R + H_{ATOM}$ will be used as the unperturbed Hamiltonian for the system. The operator $H_R + H_{ATOM}$ has the eigenfunctions

$$|\text{ATOM + PHOTONS}\rangle = |j\rangle_{ATOM} |n_1 \ldots n_\alpha \ldots\rangle_{PHOTONS} \tag{2.8}$$

where j represents any quantum numbers necessary to characterize the state of the atom. The operator H_{INT} will induce transitions between atomic states.

(b.) The Scattering Rate

Two photon processes can occur through second order transitions involving H_1 as given by Eqn. (2.6) or through first order transitions involving H_2 as given by Eqn. (2.7). The transitions involving

$a_\alpha a_{\alpha'}$ and $a^\dagger_\alpha a^\dagger_{\alpha'}$, are two-photon absorption and emission, while the transitions involving $a_\alpha a^\dagger_{\alpha'}$, and $a^\dagger_\alpha a_{\alpha'}$, are associated with scattering processes. First order scattering involving H_2 may be throught of as a direct process (i.e. one in which the absorption and emission are simultaneous processes). This is usually referred to as the Waller term (Fig. 5). In order to discuss second order scattering involving H_1 we must introduce the possibility of intermediate atomic states, considering the scattering to be a two-stage process. In our case there are two classes of such intermediate states differing in the order in which the absorption of $\hbar\omega_i$ and the emission of $\hbar\omega_f$ take place (the Kramers-Heisenberg terms in Fig. 5):

(I) $\hbar\omega_i$ is absorbed first, thus leaving no photons present in the intermediate state. In the transition to the final state $\hbar\omega_f$ is emitted.

(II) $\hbar\omega_f$ is emitted first, thus leaving two photons present in the intermediate state. In the transition to the final state $\hbar\omega_i$ is absorbed.

In both possible intermediate states the atom may be excited in any state m.

The general transition rate for inelastic photon scattering including the possibility of an ejected electron in the final state is given by Fermi's Golden Rule (neglecting any lifetime effects) taken to second order:

Figure 5 Light scattering diagram. Solid line, atom; dotted line, photons.

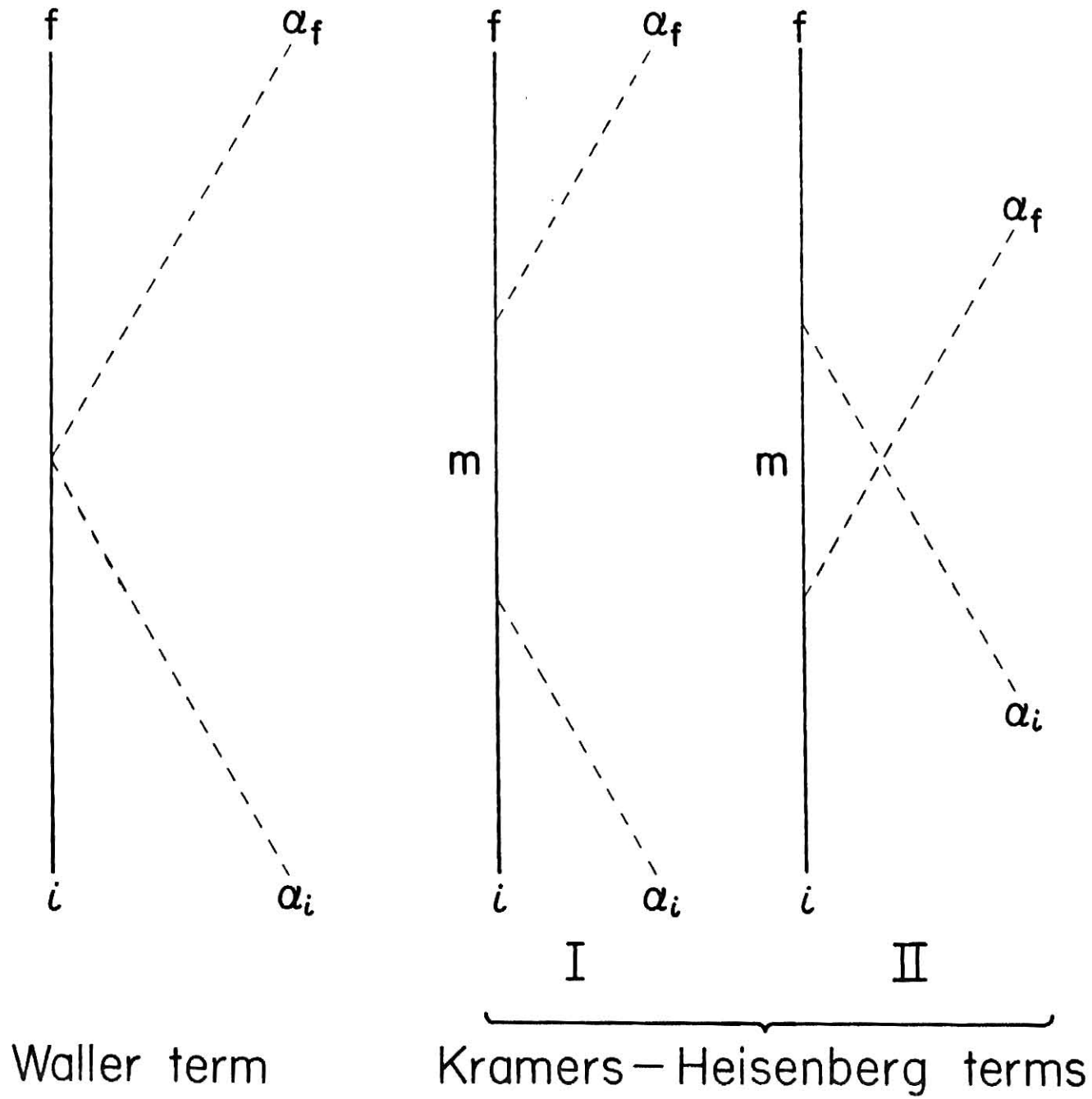
f
α_f
i
α_i
f
α_f
m
i
α_i
f
α_f
m
α_i
i
I
II
Waller term
Kramers – Heisenberg terms

$$d^4W_{if} = \frac{2\pi}{\hbar} \left| \langle F|H_2|I\rangle + \sum_M \frac{\langle F|H_1|M\rangle\langle M|H_1|I\rangle}{E_I - E_M} \right|^2$$

$$\times \rho_\varepsilon \rho_{\omega_f} \, d\varepsilon \, d\Omega_\varepsilon \, d(\hbar\omega_f) d\Omega_{\omega_f} \, \delta(E_{TOTAL_f} - E_{TOTAL_i}) \qquad (2.9)$$

where ε is the energy of the ejected electron and the initial and final states are defined by:

$$|I\rangle = |i\rangle_{ATOM} \, |\ldots n_{\alpha_i} \ldots n_{\alpha_f} \ldots\rangle_{PHOTONS}$$

$$|F\rangle = |f\rangle_{ATOM} \, |\ldots (n_{\alpha_i} - 1) \ldots (n_{\alpha_f} + 1) \ldots\rangle_{PHOTONS} \; . \qquad (2.10)$$

In the following development we will require the electron-photon system to conserve energy but not necessarily to conserve momentum (i.e. we will assume that the recoiling nucleus is capable of taking off a large amount of momentum without taking off much energy).

Using H_2 as given by Eqn. (2.7) and considering the photon field to contain the two general modes $\alpha_i = \{\bar{k}_i, \lambda_i\}$ and $\alpha_f = \{\bar{k}_f, \lambda_f\}$ (where the helicity of the photons may be either + or - in either mode) we obtain:

$$\langle F|H_2|I\rangle = \frac{e^2\hbar}{2\epsilon_o m L^3} \, \frac{\bar{e}_{\lambda_i} \cdot \bar{e}^*_{\lambda_f}}{\sqrt{\omega_i \omega_f}} \sum_j \langle f| e^{i(\bar{k}_i - \bar{k}_f)\cdot \bar{r}_j} |i\rangle$$

$$\times \sqrt{n_{\lambda_i} (n_{\lambda_f} + 1)} \; . \qquad (2.11)$$

In our particular case of silicon Kα radiation scattered by a silicon sample, we have $\hbar\omega_i = 1739$ eV and $0 \leq \hbar\omega_f \leq 1640$ eV. Thus $|(\bar{k}_i - \bar{k}_f)\cdot \bar{r}_j|_{MAX} \sim 0.03$ and $\langle F|H_2|I\rangle$ vanishes in the dipole approximation.

The summation in Eqn. (2.9) extends over all possible intermediate states. We may express the two general classes of intermediate states in the notation of Eqn. (2.10) as:

$$|M_1\rangle = |m\rangle_{ATOM}\ |\ldots(n_{\alpha_i} - 1)\ldots n_{\alpha_f}\ldots\rangle_{PHOTONS}$$

$$|M_2\rangle = |m\rangle_{ATOM}\ |\ldots n_{\alpha_i}\ldots(n_{\alpha_f} + 1)\ldots\rangle_{PHOTONS} \qquad (2.12)$$

where $|M_1\rangle$ ($|M_2\rangle$) corresponds to process I (II) in Fig. 5. Using H_1 as given by Eqn. (2.6) we obtain:

$$\langle M_1|H_1|I\rangle = \frac{e}{m}\left(\frac{\hbar}{2\epsilon_o L^3}\right)^{1/2} \frac{\sqrt{n_{\lambda_i}}}{\sqrt{\omega_i}} \langle m|\bar{e}_{\lambda_i}\cdot \sum_j \bar{p}_j\, e^{i\bar{k}_i\cdot\bar{r}_j}|i\rangle, \qquad (2.13)$$

$$\langle M_2|H_1|I\rangle = \frac{e}{m}\left(\frac{\hbar}{2\epsilon_o L^3}\right)^{1/2} \frac{\sqrt{n_{\lambda_f}+1}}{\sqrt{\omega_f}}$$

$$\times \langle m|\bar{e}^{\,*}_{\lambda_f}\cdot \sum_j \bar{p}_j\, e^{-i\bar{k}_f\cdot\bar{r}_j}|i\rangle \quad , \qquad (2.14)$$

$$\langle F|H_1|M_1\rangle = \frac{e}{m}\left(\frac{\hbar}{2\epsilon_o L^3}\right)^{1/2} \frac{\sqrt{n_{\lambda_f}+1}}{\sqrt{\omega_f}}$$

$$\times \langle f|\bar{e}^{\,*}_{\lambda_f}\cdot \sum_j \bar{p}_j\, e^{-i\bar{k}_f\cdot\bar{r}_j}|m\rangle \quad , \qquad (2.15)$$

$$\langle F|H_1|M_2\rangle = \frac{e}{m}\left(\frac{\hbar}{2\epsilon_o L^3}\right)^{1/2} \frac{\sqrt{n_{\lambda_i}}}{\sqrt{\omega_i}} \langle f|\bar{e}_{\lambda_i} \cdot \sum_j \bar{p}_j\, e^{i\bar{k}_i\cdot\bar{r}_j}|m\rangle. \quad (2.16)$$

The energy denominator in Eqn. (2.9) may be resolved as follows:

$$E_I = E_i + \hbar\omega_i$$

$$E_{M_1} = E_m$$

$$E_{M_2} = E_m + \hbar\omega_i + \hbar\omega_f \ . \quad (2.17)$$

Thus

$$E_I - E_{M_1} = E_i - E_m + \hbar\omega_i$$

$$E_I - E_{M_2} = E_i - E_m - \hbar\omega_f \quad (2.18)$$

The summation in Eqn. (2.9) may now be expressed in the dipole approximation as:

$$\sum_M \cdots = \frac{e^2}{m^2}\left(\frac{\hbar}{2\epsilon_o L^3}\right) \frac{\sqrt{n_{\lambda_i}(n_{\lambda_f}+1)}}{\sqrt{\omega_i\omega_f}}$$

$$\times \sum_m \left\{ \frac{\langle f|\bar{e}^{\,*}_{\lambda_f}\cdot\Sigma\,\bar{p}_j|m\rangle\langle m|\bar{e}_{\lambda_i}\cdot\Sigma\,\bar{p}_\ell|i\rangle}{E_i - E_m + \hbar\omega_i} \right.$$

$$\left. + \frac{\langle f|\bar{e}_{\lambda_i}\cdot\Sigma\,\bar{p}_j|m\rangle\langle m|\bar{e}^{\,*}_{\lambda_f}\cdot\Sigma\,\bar{p}_\ell|i\rangle}{E_i - E_m - \hbar\omega_f} \right\} \quad (2.19)$$

For brevity in the following discussion we will make the substitutions $\bar{P} = \sum_j \bar{p}_j$, $\bar{e}_i = \bar{e}_{\lambda_i}$ and $\bar{e}_f = \bar{e}_{\lambda_f}$. Equation (2.19) shows that the contribution of the second order term can be quite large if the incident energy $\hbar\omega_i$ is close to some energy difference $E_m - E_i$ within the atom. This occurs, for example, if $\hbar\omega_i$ is near an atomic absorption edge as is the case in resonance Raman scattering.

For our purposes we will assume the atom to be in a ^1S ground state initially. Thus, in the case of silicon, we will neglect electrons in the M shell since they do not participate in the scattering process. We will also neglect all intermediate states except those which correspond to a 1s vacancy since $\hbar\omega_i = \hbar\omega_{SiK\alpha}$ is close to the corresponding ionization energy (i.e. the first term in Eqn. (2.19) is large). Finally we will neglect the possibility of flipping the spin of the ejected electron since the Hamiltonian we have used is spin-independent. Thus the atomic states to be considered are:

$$
\begin{aligned}
|i\rangle &= {}^1S;\ (E_i) \\
|m\rangle &= (1s)^{-1}\ \varepsilon p\ {}^1P;\ (E_m = E_i + \varepsilon + \hbar\omega_k) \\
|f\rangle &= (2p)^{-1}\ \varepsilon p\ {}^1S,\ {}^1P,\ {}^1D;\ (E_f = E_i + \varepsilon + \hbar\omega_L)
\end{aligned}
\qquad (2.20)
$$

where ε is taken to be the same in the intermediate and final states and multiplet splitting has been ignored. If we neglect the second (non-resonant) term in Eqn. (2.19) and consider the summation to be a sum over m_L' states of the intermediate state we obtain:

$$\sum_{M} \cdots = \frac{e^2}{m^2} \left(\frac{1}{2\epsilon_o L^3}\right) \frac{\sqrt{n_{\lambda_i}(n_{\lambda_f}+1)}}{\sqrt{\omega_i \omega_f}}$$

$$\times \sum_{m_L'} \frac{\langle f|\bar{e}_f^* \cdot \bar{P}|m\rangle\langle m|\bar{e}_i \cdot \bar{P}|i\rangle}{\omega_i - \omega_k - \omega} \qquad (2.21)$$

where $\omega = \varepsilon/\hbar$. The matrix elements are given by:

$$\langle f|\bar{e}_f^* \cdot \bar{P}|m\rangle = \langle f\ell_1\ell_2 L m_L|\bar{e}_f^* \cdot \bar{P}|m\ell_1'\ell_2' L' m_L'\rangle \quad ,$$

$$\langle m|\bar{e}_i \cdot P|i\rangle = \langle mL'm_L'|\bar{e}_i \cdot \bar{P}|iL''m_L''\rangle \qquad (2.22)$$

where ℓ_1 refers to the atom and ℓ_2 refers to the ejected electron.

For the moment we will confine our attention to reducing the expression:

$$M_{IF} = \sum_{m_L'} \langle f|\bar{e}_f^* \cdot \bar{P}|m\rangle\langle m|\bar{e}_i \cdot \bar{P}|i\rangle \quad . \qquad (2.23)$$

Using $\bar{e}_f^* \cdot \bar{P} = \sum_q P_q(\bar{e}_f^* \cdot \bar{e}_q^*)$ where the $\bar{e}_q$ are spherical unit vectors we may expand the first expression in Eqn. (2.22) to yield:

$$\langle f|\bar{e}_f^{*}\cdot\bar{P}|m\rangle = \sum_{\substack{q\, m_1\\ m_2 m_1'}} (-)^{2\ell_2-m_1+m_L-\ell_1'+m_L'}[(2L+1)(2L'+1)]^{1/2}(\bar{e}_f^{*}\cdot\bar{e}_q^{*})$$

$$\times \begin{pmatrix} \ell & \ell & L \\ m_1 & m_2 & -m_L \end{pmatrix} \begin{pmatrix} \ell_1' & \ell_2 & L' \\ m_1' & m_2 & -m_L' \end{pmatrix} \begin{pmatrix} \ell_1 & 1 & \ell_1' \\ -m_1 & q & m_1' \end{pmatrix}$$

$$\times \langle f\ \ell_1 \| \bar{P} \| m\ \ell_1'\rangle \tag{2.24}$$

where we have assumed that $\bar{P}_q^K$ commutes with the ℓ_2,ℓ_2' part of the wave functions (i.e. the ejected electron is not affected in the transition $|m\rangle \rightarrow |f\rangle$). If we substitute $\ell_1 = \ell_2 = \ell_2' = L' = 1$, $\ell_1' = m_1' = 0$ and make use of the symmetry properties of the 3-j symbols Eqn. (2.24) reduces to:

$$\langle f|\bar{e}_f^{*}\cdot\bar{P}|m\rangle = \frac{(2L+1)^{1/2}}{\sqrt{3}} \sum_q (-)^{m_L}(\bar{e}_f^{*}\cdot\bar{e}_q^{*}) \begin{pmatrix} 1 & 1 & L \\ q & m_L' & -m_L \end{pmatrix}$$

$$\times \langle f\ 1 \| \bar{P} \| m\ 0\rangle \quad . \tag{2.25}$$

The second expression in Eqn. (2.22) may be expanded to yield ($L'' = m_L'' = 0$):

$$\langle m|\bar{e}_i\cdot\bar{P}|i\rangle = \sum_{q'} (-)^{1-m_L'}(\bar{e}_i\cdot\bar{e}_{q'}^{*}) \begin{pmatrix} 1 & 1 & 0 \\ -m_L' & q' & 0 \end{pmatrix}$$

$$\times \langle m\ 1 \| \bar{P} \| i\ 0\rangle \quad . \tag{2.26}$$

Combining Eqns. (2.25) and (2.26) we obtain:

$$M_{IF} = \frac{(2L+1)^{1/2}}{\sqrt{3}} \langle f\ 1 \| \bar{P} \| m\ 0 \rangle \langle m\ 1 \| \bar{P} \| i\ 0 \rangle$$

$$\times \sum_{m_L' q q'} (-)^{1+m_L-m_L'} (\bar{e}_f^* \cdot \bar{e}_q^*)(\bar{e}_i \cdot \bar{e}_{q'}^*)$$

$$\times \begin{pmatrix} 1 & 1 & L \\ q & q' & -m_L \end{pmatrix} \begin{pmatrix} 1 & 1 & 0 \\ -m_L' & q' & 0 \end{pmatrix}$$

$$= \frac{(2L+1)^{1/2}}{3} \langle f\ 1 \| \bar{P} \| m\ 0 \rangle \langle m\ 1 \| \bar{P} \| i\ 0 \rangle$$

$$\times (-)^{m_L} \sum_{q q'} (\bar{e}_f^* \cdot \bar{e}_q^*)(\bar{e}_i \cdot \bar{e}_{q'}^*) \begin{pmatrix} 1 & 1 & L \\ q & q' & -m_L \end{pmatrix} \qquad (2.27)$$

thus establishing $m_L' = q'$ as the only non-zero term in $\sum_{m_L'} \cdots$. Multiplying Eqn. (2.27) by its complex conjugate gives:

$$|M_{IF}|^2 = \frac{(2L+1)}{9} \left|\langle f\ 1 \| \bar{P} \| m\ 0 \rangle\right|^2 \left|\langle m\ 1 \| \bar{P} \| i\ 0 \rangle\right|^2$$

$$\times \sum_{\substack{q\ q'' \\ q' q'''}} (\bar{e}_f^* \cdot \bar{e}_q^*)(\bar{e}_f \cdot \bar{e}_{q''})(\bar{e}_i \cdot \bar{e}_{q'}^*)(\bar{e}_i^* \cdot \bar{e}_{q'''})$$

$$\times \begin{pmatrix} 1 & 1 & L \\ q & q' & -m_L \end{pmatrix} \begin{pmatrix} 1 & 1 & L \\ q'' & q''' & -m_L \end{pmatrix}$$

$$|M_{IF}|^2 = \frac{(2L+1)}{9} |\langle f\ 1 \| \bar{P} \| m\ 0\rangle|^2\ |\langle m\ 1 \| \bar{P} \| i\ 0\rangle|^2$$

$$\times \sum_{q'q'''} \beta_{f_{(m_L-q')}} \beta^*_{f_{(m_L-q''')}} \beta_{i_{q'}} \beta^*_{i_{q'''}}$$

$$\times \begin{pmatrix} 1 & 1 & L \\ q' & (m_L-q') & -m_L \end{pmatrix} \begin{pmatrix} 1 & 1 & L \\ q''' & (m_L-q''') & -m_L \end{pmatrix} \qquad (2.28)$$

where again we have used the symmetry properties of the 3-j symbols to eliminate the summations over q and q". We have also made substitutions of the form $\beta_{i_{q'}} \equiv (\bar{e}_i \cdot \bar{e}^*_{q'})$. If we assume the initial photons to have circular polarization with polarization vectors given by:

$$\bar{e}_i^{(\pm)} = \mp \frac{1}{\sqrt{2}} (\bar{e}_x \pm i\bar{e}_y) \qquad (2.29)$$

and with $\hat{k}_i = \hat{e}_z = \hat{e}_0$, then it can be shown that the summation $\sum_{q'q'''} \cdots$ contains only two non-vanishing terms:

$$\sum_{q'q'''} \cdots = |\beta_{f_{(m_L-1)}}|^2 \begin{pmatrix} 1 & 1 & L \\ 1 & (m_L-1) & -m_L \end{pmatrix}^2 \begin{Bmatrix} 1 & (+)_i \\ 0 & (-)_i \end{Bmatrix}$$

$$+ |\beta_{f_{(m_L+1)}}|^2 \begin{pmatrix} 1 & 1 & L \\ -1 & (m_L+1) & -m_L \end{pmatrix}^2 \begin{Bmatrix} 0 & (+)_i \\ 1 & (-)_i \end{Bmatrix} . \qquad (2.30)$$

We must now compute the quantities $|\beta_{f_1}|^2$, $|\beta_{f_0}|^2$, $|\beta_{f_{-1}}|^2$. We will suppose an alignment of coordinate systems O_{xyz} (initial) and

$O_{x'y'z'}$ (final) such that $\hat{k}_f = \hat{e}_{z'}$, and the z, z', x, and x' axes all lie in the same plane. Then the transformation from unprimed to primed coordinate systems is accomplished by a rotation about the y axis ($\hat{e}_y = \hat{e}_{y'}$). The rotation matrix is given by:

	x	y	z
x'	cos θ	0	-sin θ
y'	0	1	0
z'	sin θ	0	cos θ

. (2.31)

If we assume the scattered photons to have circular polarization of the form (2.29) in the primed coordinate system then a simple transformation gives:

$$\bar{e}_f^{(\pm)} = \mp \frac{1}{\sqrt{2}} (\cos\theta\ \bar{e}_x \pm i\ \bar{e}_y - \sin\theta\ \bar{e}_z) \quad . \tag{2.32}$$

We then obtain:

$$\begin{aligned} |\beta_{f_1}|^2 &= \frac{1}{4} (\cos^2\theta \mp 2\cos\theta + 1) \quad , \\ |\beta_{f_0}|^2 &= \frac{1}{2} \sin^2\theta \quad , \\ |\beta_{f_{-1}}|^2 &= \frac{1}{4} (\cos^2\theta \pm 2\cos\theta + 1) \end{aligned} \tag{2.33}$$

where the upper (lower) sign is to be taken for $(+)_f$ ($(-)_f$).

Since the incident beam of Kα x rays is assumed to have zero net polarization (i.e. equal numbers of $(+)_i$ and $(-)_i$ photons), and the

final polarization is not measured in this experiment we must average over the two possible initial polarization states and sum over the two possible final polarization states. Thus:

$$|M_{IF}|^2_{TOTAL} = \frac{1}{2}\left\{|(+)_i \to (+)_f|^2 + |(+)_i \to (-)_f|^2 + |(-)_i \to (+)_f|^2 + |(-)_i \to (-)_f|^2\right\} \tag{2.34}$$

where the $|(\pm)_i \to (\pm)_f|^2$ terms simply represent $|M_{IF}|^2$ (Eqn. (2.28) with the appropriate choice of $\bar{e}_i^{(\pm)}$ and $\bar{e}_f^{(\pm)}$.

Finally, combining the results of Eqn.s (2.33), (2.30), (2.28), and (2.34) and summing over all allowed L and m_L values of the final state, we obtain after some algebra:

$$\sum_{L,m_L} |M_{IF}|^2_{TOTAL} = \frac{2}{9}\,|\langle f\ 1 \| \bar{P} \| m\ 0\rangle|^2\ |\langle m\ 1 \| \bar{P} \| i\ 0\rangle|^2$$

$$= 2|\langle f\ 1\ 0|\ P_z\ |m\ 0\ 0\rangle|^2\ |\langle m\ 1\ 0|\ P_z\ |i\ 0\ 0\rangle|^2 . \tag{2.35}$$

In each of the transitions indicated in Eqn. (2.35) only a single electron has changed its orbital. In the case of $\langle m\ 1\ 0|\ P_z\ |i\ 0\ 0\rangle$ a 1s electron makes the transition 1s → εp while in $\langle f\ 1\ 0|\ P_z\ |m\ 0\ 0\rangle$ a 2p electron makes the transition 2p → 1s. Thus if we substitute Slater determinants for the true atomic wave functions in Eqn. (2.35) it can be shown that:

$$\langle m\ 1\ 0|\ P_z\ |i\ 0\ 0\rangle = \langle m\ 1\ 0|\ \sum_j p_{z_i}\ |i\ 0\ 0\rangle$$

$$= \langle \varepsilon p|\ p_z\ |1s\rangle \qquad (2.36)$$

and likewise

$$\langle f\ 1\ 0|\ P_z\ |m\ 0\ 0\rangle = \langle 1s|\ p_z\ |2p\rangle \qquad (2.37)$$

where the wave functions have been reduced to single electron wave functions. Note that in Eqn. (2.37) the 1s wave function is calculated in the presence of a 2p vacancy and, likewise, the 2p wave function is calculated in the presence of a 1s vacancy. For convenience we will choose the continuum electron wave function in Eqn. (2.36) to be normalized per unit energy interval.

The general transition rate (Eqn. (2.9)) may now be written in terms of the single electron wave functions by combining the results of Eqns. (2.37), (2.36), (2.35), and (2.21) to yield:

$$d^3W_{if} = \frac{2\pi}{\hbar}\left(\frac{e^2}{2m^2\epsilon_o L^3}\right)^2 \frac{n_i(n_f+1)}{\omega_i\omega_f}\ \frac{(2)|\langle 1s|p_z|2p\rangle|^2|\langle \varepsilon p|p_z|1s\rangle|^2}{(\omega_k+\omega-\omega_i)^2}$$

$$\times\ \rho_{\omega_f}\ d\varepsilon\ d(\hbar\omega_f)\ d\Omega_{\omega_f}\ \delta(\hbar\omega_i-\hbar\omega_f-\hbar\omega-\hbar\omega_L) \qquad (2.38)$$

where we have integrated over $d\Omega_\varepsilon$. The factor $4\pi\rho_\varepsilon$ does not explicitly appear in Eqn. (2.38) due to our choice of normalization for $|\varepsilon p\rangle$ (i.e. this factor has now been included in the normalization constant for $|\varepsilon p\rangle$).

If we substitute $\rho_{\omega_f} = L^3\omega_f^2/\hbar(2\pi c)^3$ for the scattered photon density of final states in Eqn. (2.38) we obtain:

$$d^3W_{if} = \frac{2r_o^2}{m^2\hbar^2}\,\frac{\omega_f}{\omega_i}\,\frac{cn_i(n_f+1)}{L^3}\,\frac{|\langle 1s|p_z|2p\rangle|^2\,|\langle \varepsilon p|p_z|1s\rangle|^2}{(\omega_k+\omega-\omega_i)^2}$$

$$\times\,\delta(\omega_i-\omega_f-\omega-\omega_L)d\varepsilon\,d\omega_f\,d\Omega_{\omega_f} \qquad (2.39)$$

where $r_o = e^2/4\pi\epsilon_o mc^2$ is the classical electron radius. The transition rate is proportional to the number of initial photons in the field, n_i, as expected and consists of two terms. The term which is proportional to n_f represents the rate of <u>induced</u> scattering while the term which is independent of n_f represents the rate of <u>spontaneous</u> scattering. For a radiation field in thermal equalibrium Planck's law gives $(n_f)_{AVE} = (\exp(\hbar\omega_f/kT) - 1)^{-1}$. In our case $\hbar\omega_f \lesssim 1640$ eV which means that $\hbar\omega_f/kT \gg 1$ for temperatures $\lesssim 10^6$ °K. Thus $(n_f)_{AVE} \sim 0$ and it is sufficient to consider only the rate due to spontaneous scattering.

We may relate the scattering rate given by Eqn. (2.39) to the K absorption cross section per atom by observing that for an arbitrary initial photon energy $\hbar\omega'_i$ we have:

$$d\sigma_k(\omega'_i) = \frac{2\pi e^2}{m^2\epsilon_o\omega'_i c}\,|\langle\varepsilon' p|p_z|1s\rangle|^2\,\delta(\hbar\omega'_i-\hbar\omega_k-\varepsilon')d\varepsilon' \qquad (2.40)$$

where again $|\varepsilon' p\rangle$ has been normalized per unit energy interval. Upon integration over $d\varepsilon'$ we obtain:

$$\sigma_k(\omega'_i) = \frac{2\pi e^2}{m^2 \epsilon_o c \omega'_i} \left|\langle \varepsilon' p | p_z | 1s \rangle\right|^2 \tag{2.41}$$

where now $\varepsilon' = \hbar\omega'_i - \hbar\omega_k$. If we substitute $\hbar\omega'_i = \hbar\omega_k + \varepsilon$ in Eqn. (2.41) we have $\varepsilon' = \varepsilon$ and thus:

$$\sigma_k(\omega_k + \omega) = \frac{8\pi^2 \alpha \hbar}{m^2(\omega_k + \omega)} \left|\langle \varepsilon p | p_z | 1s \rangle\right|^2$$

where we have introduced the fine structure constant $\alpha = e^2/4\pi\epsilon_o\hbar c$. The scattering rate in Eqn. (2.39) may now be written as:

$$d^3W_{if} = \frac{r_o^2}{4\pi^2\alpha\hbar^3} \frac{\omega_f}{\omega_i} \frac{cn_i}{L^3} \frac{(\omega_k+\omega)\sigma_k(\omega_k+\omega)\left|\langle 1s | p_z | 2p \rangle\right|^2}{(\omega_k + \omega - \omega_i)^2}$$

$$\times \delta(\omega_i - \omega_f - \omega - \omega_L) d\varepsilon \, d\omega_f \, d\Omega_{\omega_f} \quad . \tag{2.43}$$

Integrating Eqn. (2.43) over $d\varepsilon$ and $d\Omega_{\omega_f}$ we obtain:

$$dW_{if} = \frac{r_o^2}{\pi\alpha\hbar^2} \frac{\omega_f}{\omega_i} \frac{cn_i}{L^3} \frac{(\omega_{k\alpha}+\omega_i-\omega_f)}{(\omega_{k\alpha}-\omega_f)^2} \sigma_k(\omega_{k\alpha}+\omega_i-\omega_f)$$

$$\times \left|\langle 1s | p_z | 2p \rangle\right|^2 d\omega_f \quad . \tag{2.44}$$

Finally, dividing Eqn. (2.44) by the incident photon flux $\Phi = cn_i/L^3$ and multiplying by 2 to account for the two possible spin states of the ejected electron we obtain an expression for the energy differential cross section per atom associated with the resonant Raman scattering process:

$$d\sigma_{RS}(\omega_i) = \frac{2}{\Phi} dW_{if}$$

$$= \frac{2r_o^2}{\pi\alpha\hbar^2} \frac{\omega_f}{\omega_i} \frac{(\omega_{k\alpha}+\omega_i-\omega_f)}{(\omega_{k\alpha}-\omega_f)^2} \sigma_k(\omega_{k\alpha}+\omega_i-\omega_f)$$

$$\times |\langle 1s|p_z|2p\rangle|^2 d\omega_f \quad . \tag{2.45}$$

Note that this expression includes only the resonant part of the scattering cross section. Recent work by J. Tulkki and T. Åberg[11] has shown that inclusion of the second (non-resonant) term in Eqn. (2.19) results in the addition of a small anisotropic contribution to the scattering cross section $d^2\sigma_{RS}/d\Omega_{\omega_f} d\omega_f$. Numerically, they estimate that this contribution does not change $d^2\sigma_{RS}/d\Omega_{\omega_f} d\omega_f$ by more than about 10%. Thus, for our purposes, we will choose to neglect the contribution of the non-resonant term. The total resonant contribution to the cross section is obtained by integrating Eqn. (2.45) over ω_f which varies from 0 to $\omega_i - \omega_L$.

The differential cross section as given by Eqn. (2.45) is still general to the extent that ω_i remains unspecified. The only restriction on ω_i is that it be such that the resonance condition can be met (i.e. the first term in Eqn. (2.19) is dominant) and yet lifetime effects for the K hole state can be neglected (i.e. $(\omega_i - \omega_k)^2 >> \Gamma_k^2/4\hbar^2$ where Γ_k is the line width associated with the K hole state). Additionally, Z_{Target} should be ≥ 10 in order to justify our assumption of a filled L shell.

The energy profile of $d\sigma_{RS}/dE_f$ for silicon Kα radiation on solid silicon is shown in Fig. 6 for the energy range $1540 \leq E_f \leq 1640$ eV.

Figure 6 Energy profile for resonance Raman process (based on Eqn. (2.45)).

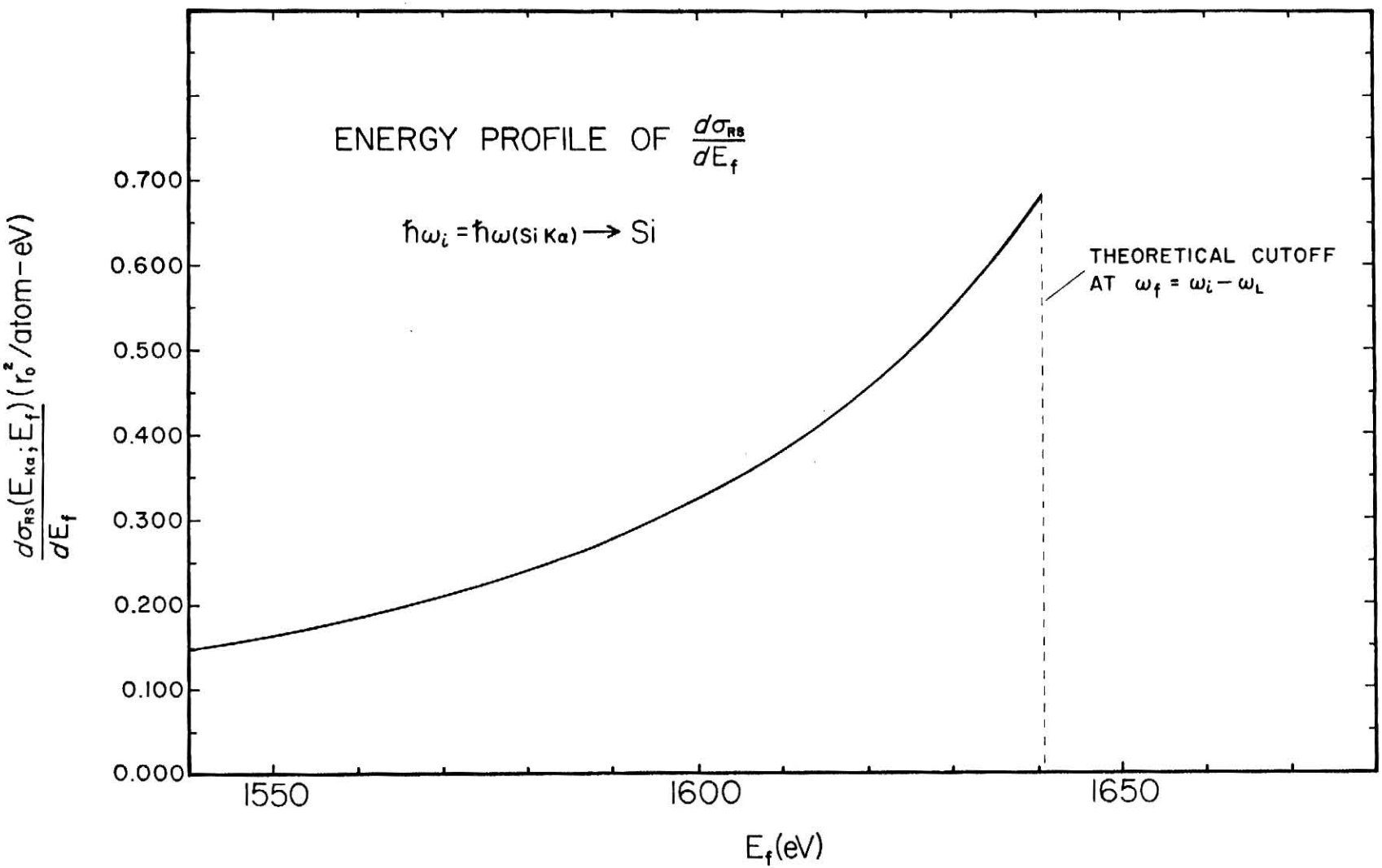
ENERGY PROFILE OF $\frac{d\sigma_{RS}}{dE_f}$
$\hbar\omega_i = \hbar\omega(\text{Si K}\alpha) \longrightarrow$ Si
THEORETICAL CUTOFF
AT $\omega_f = \omega_i - \omega_L$
$\frac{d\sigma_{RS}(E_{K\alpha};E_f)}{dE_f}(r_o^2/\text{atom-eV})$
0.700
0.600
0.500
0.400
0.300
0.200
0.100
0.000
1550
1600
1650
E_f(eV)

THICK TARGET ANALYSIS

In this section we will consider the resonant Raman scattering of characteristic Kα photons within a thick solid target. The photons are produced as a result of K ionization produced by ion bombardment. The incident ions will be treated as a parallel beam of arbitrary cross section. The intensity of the beam is described by the number I_o of monoenergetic ions, energy E, per unit time which pass through a unit area normal to the beam direction. The incident beam makes an angle α with the normal to the target surface as shown in Fig. 7. Neglecting losses due to straggling[14] and small angle scattering,[15] the rate of ions impinging on a differential element of surface area dA' located parallel to the surface is approximately independent of depth up to the ion range and is given by:

$$I_o \, dA' \cos\alpha \tag{3.1}$$

The rate of Kα photon production within a volume element $dV' = (dA'\cos\alpha)ds' = dA'\, dt'$ at a target depth t' (point A on Fig. (7)) is given by:

$$I_o \, dV' \, n\sigma_{KX}(E(s')) \tag{3.2}$$

where n is the atomic density of the target, σ_{KX} is the K x-ray production cross section (equal to the K-shell fluorescence yield times the K ionization cross section σ_I), $s' = t'/\cos\alpha$ is the linear penetration depth of the ion beam, and E(s') is the ion energy at depth s'.

Figure 7 Target geometries used in thick target analysis of Section III.

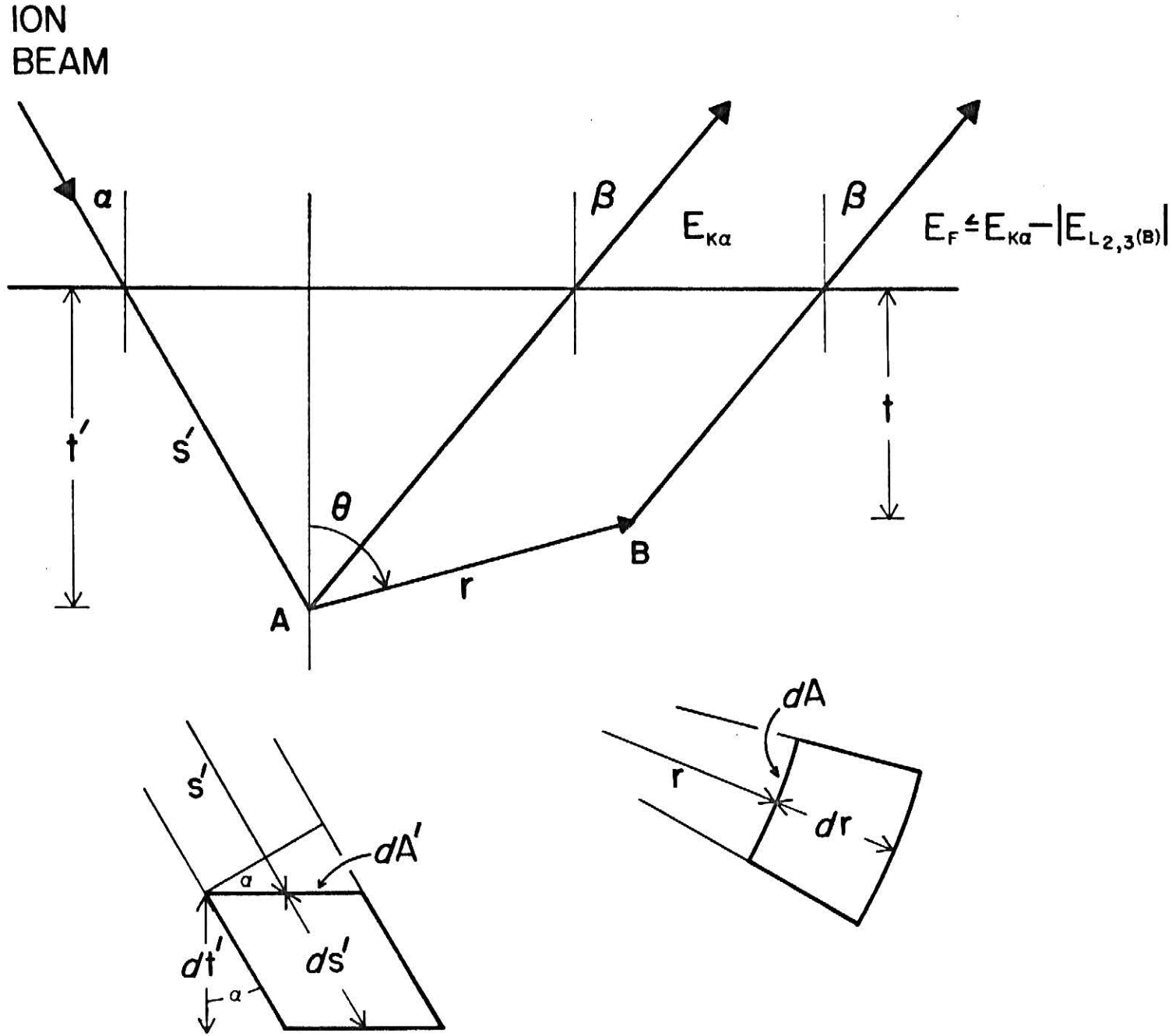
ION
BEAM
α
β
$E_{K\alpha}$
β
$E_F \triangleq E_{K\alpha} - |E_{L_{2,3}(B)}|$
t′
s′
θ
A
r
B
t
s′
dA′
α
dt′
ds′
α
dA
r
dr

The intensity of these Kα photons on the surface of an imaginary sphere of radius r centered at dV' may be written as:

$$I' \equiv I_o \, dV' \, n\sigma_{KX}(s') \, \frac{e^{-\mu_2 r}}{4\pi r^2} \tag{3.3}$$

where $\mu_2 = \mu_2(E_{K\alpha})$ is the linear absorption coefficient for Kα radiation. Using this we may calculate the rate at which photons from dV' enter the spherical volume element dV (point B on Fig. 7) and are scattered into an energy interval $(E_f, E_f + dE_f)$ through the resonant Raman process:

$$I' \, dV \, n \, d\sigma_{RS}(E_{K\alpha};E_f) \quad . \tag{3.4}$$

Here $d\sigma_{RS}(E_{K\alpha};E_f)$ (see Section II, Eqn. (2.45)) refers to a differential segment of σ_{RS} responsible for scattering incident radiation ($E_i = E_{K\alpha}$) into the interval $(E_f, E_f + dE_f)$. Finally, the rate at which Raman scattered photons from dV reach the detector is given by:

$$I' \, dV \, n \, d\sigma_{RS} \, e^{-\mu_3 t/\cos\beta} \, (d\Omega_\beta/4\pi)$$

$$= I_o \frac{dV'}{4\pi} \frac{dV}{r^2} n^2 \, \sigma_{KX}(s') \, d\sigma_{RS}(d\Omega_\beta/4\pi) \, e^{-\mu_2 r - \mu_3 t/\cos\beta} \tag{3.5}$$

where $d\Omega_\beta$ is the solid angle subtended at dV by the detector (or spectrometer image slit) and $\mu_3 = \mu_3(E_f)$ is the linear absorption coefficient for the scattered radiation. Based on the theoretical development of Section II we have assumed that the scattered radiation is emitted isotropically from dV.

Integration of Eqn. (3.5) over the sample volume (with origin at dV') gives the total detectable Raman yield (E_f component) due to Kα radiation from dV'. For a distant detector (or spectrometer image slit) we will assume that the solid angle factor $d\Omega_\beta/4\pi$ is approximately constant (to within ∿ 1%) and that it may be moved outside of the integral to yield:

$$R(dV';E_f) \equiv I_o \frac{dV'}{4\pi} n^2 \sigma_{KX}(s') \, d\sigma_{RS} \, (d\Omega_\beta/4\pi)$$

$$\times \int_V e^{-\mu_2 r - \mu_3 t/\cos\beta} \sin\theta \, d\theta \, d\phi \, dr \quad . \tag{3.6}$$

A factor K is defined to be

$$K \equiv I_o \frac{dV'}{2} n^2 \, d\sigma_{RS}(d\Omega_\beta/4\pi)$$

and it is noted that $t = t' - r\cos\theta$ so that Eqn. (3.6) can be written as:

$$R(dV';E_f) = K \, \sigma_{KX}(s') \, e^{-\mu_3 t'/\cos\beta} \int_{(r)} \int_{(\theta)} e^{\mu_3 r\cos\theta/\cos\beta - \mu_2 r}$$

$$\times \sin\theta \, d\theta \, dr \tag{3.7}$$

where we have integrated over dϕ. For convenience the region of integration over r and θ may be divided into two parts: (1) a sphere of radius t' centered at dV' and (2) the remaining sample volume outside

of the sphere. Then we obtain:

$$R(dV';E_f) = K\,\sigma_{KX}(s')\,e^{-\mu_3 t'/\cos\beta}\left\{\int_0^{t'}\int_{-1}^{1} e^{\mu_3 r\cos\theta/\cos\beta-\mu_2 r} \times d(\cos\theta)dr + \int_{t'}^{\infty}\int_{-1}^{\frac{t'}{r}} e^{\mu_3 r\cos\theta/\cos\beta-\mu_2 r}\, d(\cos\theta)dr\right\}. \tag{3.8}$$

The infinite limit appearing in the r integral of the second term implies a sample which is assumed to be semi-infinite for purposes of Kα photon absorption.

Eqn. (3.8) can be integrated over the range of the ion beam to obtain the total detectable Raman yield (E_f component) due to Kα radiation from a column of differential cross section dA'cosα along the beam path. The volume element dV' contained in the constant K may be expanded into the form dV' = dA' dt' = dA'cosα ds'. Thus we have:

$$R(\alpha,\beta;E_f) = I_o\,\frac{dA'}{2}\,n^2 d\sigma_{RS}(d\Omega_\beta/4\pi)\cos\alpha \int_0^{\text{Range}} \sigma_{KX}(s')\,e^{-\mu_3 t'/\cos\beta} \times \left\{\int_0^{t'}\int_{-1}^{1} e^{\mu_3 r\cos\theta/\cos\beta-\mu_2 r}\, d(\cos\theta)dr + \int_{t'}^{\infty}\int_{-1}^{\frac{t'}{r}} e^{\mu_3 r\cos\theta/\cos\beta-\mu_2 r}\, d(\cos\theta)dr\right\} ds'$$

$$= I_o \frac{dA'}{2} n^2 d\sigma_{RS} (d\Omega_\beta/4\pi) \int_o^{(\text{Range})\cos\alpha} \sigma_{KX}(t'/\cos\alpha)\, e^{-\mu_3 t'/\cos\beta}$$

$$\times \left\{ \int_o^{t'} \int_{-1}^{1} e^{\mu_3 r\cos\theta/\cos\beta - \mu_2 r}\, d(\cos\theta)dr \right.$$

$$\left. + \int_{t'}^{\infty} \int_{-1}^{\frac{t'}{r}} e^{\mu_3 r\cos\theta/\cos\beta - \mu_2 r}\, d(\cos\theta)dr \right\} dt' \quad . \tag{3.9}$$

This expression may be evaluated numerically. The details will be dealt with in the next section.

The next step involves the determination of the Kα x-ray yield from the differential column discussed above. The detectable Kα photon yield from the volume element dV' is given by:

$$I_o\, dV'\, n\sigma_{KX}(s')(d\Omega_\beta/4\pi)\, e^{-\mu_2 t'/\cos\beta} \quad . \tag{3.10}$$

The total detectable yield from the column may now be found by integration along the beam path:

$$F(\alpha,\beta) \equiv I_o\, dA'\, \cos\alpha\, n(d\Omega_\beta/4\pi) \int_o^{\text{Range}} \sigma_{KX}(s')\, e^{-\mu_2 t'/\cos\beta}\, ds'$$

$$= I_o\, dA'\, n(d\Omega_\beta/4\pi) \int_o^{(\text{Range})\cos\alpha} \sigma_{KX}(t'/\cos\alpha)\, e^{-\mu_2 t'/\cos\beta}\, dt' \quad . \tag{3.11}$$

This expression must also be evaluated numerically due to the lack of a

simple algebraic form for $\sigma_{KX}(t'/\cos\alpha)$.

The ratio of $R(\alpha,\beta;E_f)$ to $F(\alpha,\beta)$ now provides a measure of the relative yield of Raman scattered (E_f component) to Kα radiation for a given α and β due to a single differential column along the beam path:

$$\frac{R(\alpha,\beta;E_f)}{F(\alpha,\beta)} = \frac{(I_o \frac{dA'}{2} n^2 d\sigma_{RS}(d\Omega_\beta/4\pi))}{(I_o\, dA'\, n(d\Omega_\beta/4\pi))} \frac{I_R(\alpha,\beta;E_f)}{I_F(\alpha,\beta)}$$

$$= \frac{n\, d\sigma_{RS}}{2} \frac{I_R(\alpha,\beta;E_f)}{I_F(\alpha,\beta)} \tag{3.12}$$

where

$$I_R(\alpha,\beta;E_f) \equiv \int_o^{(\text{Range})\cos\alpha} \sigma_{KX}(t'/\cos\alpha)\, e^{-\mu_3 t'/\cos\beta}$$

$$\times \left\{ \int_o^{t'} \int_{-1}^{1} e^{\mu_3 r\cos\theta/\cos\beta - \mu_2 r}\, d(\cos\theta)dr \right.$$

$$\left. + \int_{t'}^{\infty} \int_{-1}^{\frac{t'}{r}} e^{\mu_3 r\cos\theta/\cos\beta - \mu_2 r}\, d(\cos\theta)dr \right\} dt' \tag{3.13}$$

and

$$I_F(\alpha,\beta) \equiv \int_o^{(\text{Range})\cos\alpha} \sigma_{KX}(t'/\cos\alpha)\, e^{-\mu_2 t'/\cos\beta}\, dt' \quad . \tag{3.14}$$

Since all differential columns along the beam path are assumed to be identical in this model, Eqn. (3.12) also represents the total measured relative yield of Raman scattered (E_f component) to Kα radiation.

For later convenience in numerical handling Eqn. (3.12) may be modified such that all distances are in mg/cm^2 and all linear absorption coefficients (cm^{-1}) are changed to mass absorption coefficients (cm^2/mg). By making the substitutions $r(cm) = r(mg/cm^2)/\rho$, $t'(cm) = t'(mg/cm^2)/\rho$, and $\mu(cm^{-1}) = \mu(cm^2/mg)\rho$ where ρ is the target mass density in mg/cm^3 we obtain:

$$I_R(\alpha,\beta;E_f) \rightarrow \frac{1}{\rho^2} I_R(\alpha,\beta;E_f) \tag{3.15}$$

$$I_F(\alpha,\beta) \rightarrow \frac{1}{\rho} I_F(\alpha,\beta) \quad . \tag{3.16}$$

Thus we have:

$$\frac{R(\alpha,\beta;\ E_f)}{F(\alpha,\beta)} \rightarrow \frac{n}{2\rho}\ d\sigma_{RS}\ \frac{I_R(\alpha,\beta;E_f)}{I_F(\alpha,\beta)}$$

$$= \frac{N_A}{2A_m}\ d\sigma_{RS}\ \frac{I_R(\alpha,\beta;E_f)}{I_F(\alpha,\beta)} \tag{3.17}$$

where N_A is Avogadro's number and A_m is the target atomic mass. Finally, we may define a relative x-ray production efficiency ξ for the E_f component of Raman scattered radiation versus Kα radiation:

$$\xi(\alpha,\beta;E_o,E_f) = \frac{N_A}{2A_m} \frac{I_R(\alpha,\beta;E_f)}{I_F(\alpha,\beta)} \sigma_{KX}(E_o) \quad . \tag{3.18}$$

We then have:

$$\frac{R(\alpha,\beta;E_f)}{F(\alpha,\beta)} = \frac{d\sigma_{RS}(E_{K\alpha};E_f)}{\sigma_{KX}(E_o)} \xi(\alpha,\beta;E_o,E_f) \quad . \tag{3.19}$$

If the analytical shape and background of the Raman edge are known, it is possible to extract an estimate of the total integrated intensity $R(\alpha,\beta)$ associated with the resonant Raman process. Eqn. (3.19) may then be used to estimate the total cross section $\sigma_{RS}(E_i = E_{K\alpha})$ for scattering into all angles and all allowed energies ($0 \leq E_f \leq E_K - E_{L_{2,3}}$(Binding)). Care must be taken in the evaluation of $\xi(\alpha,\beta;E_o,E_f)$. The integral $I_R(\alpha,\beta;E_f)$ must effectively be integrated over E_f. Given a reasonably extensive table of mass absorption coefficients (Ref. (16) for example) this is not too difficult.

As a simple cross check of the above derivation (independent of the assumptions made therein) we may evaluate the gross x-ray yields in terms of "escape efficiencies" for the Raman scattered and characteristic radiation. The measurable characteristic x-ray yield will be given by:

$$F(\text{MEAS}) = \varepsilon_X \, F(\text{TOTAL}) \tag{3.20}$$

where $\varepsilon_X \leq 0.5$ is the escape efficiency of the characteristic target K x rays. Likewise:

$$R(MEAS;E_F) = \varepsilon_R \, R(TOTAL;E_f) \tag{3.21}$$

where $\varepsilon_R \leq 0.5$ is the escape efficiency of the Raman scattered radiation. $R(TOTAL;E_f)$ is given by:

$$R(TOTAL;E_f) = (1 - \varepsilon_X) \frac{d\sigma_{RS}}{\sigma_{ABS}} \, F(TOTAL) \tag{3.22}$$

where $(1 - \varepsilon_X)$ represents the fraction of the total characteristic radiation which is absorbed in the solid and $d\sigma_{RS}/\sigma_{ABS}$ is the fraction of the absorbed radiation which scatters into $(E_f, E_f + dE_f)$ via the resonant Raman process. Thus we have:

$$\begin{aligned} R(MEAS;E_f) &= \varepsilon_R(1 - \varepsilon_X) \frac{d\sigma_{RS}}{\sigma_{ABS}} F(TOTAL) \\ &= \frac{\varepsilon_R}{\varepsilon_X} (1 - \varepsilon_X) \frac{d\sigma_{RS}}{\sigma_{ABS}} F(MEAS) \, . \end{aligned} \tag{3.23}$$

Taking the ratio of $R(MEAS;E_f)$ to $F(MEAS)$ we obtain:

$$\begin{aligned} \frac{R(MEAS;E_f)}{F(MEAS)} &= \frac{\varepsilon_R}{\varepsilon_X} (1 - \varepsilon_X) \frac{d\sigma_{RS}}{\sigma_{ABS}} \\ &= \xi(E_o) \frac{d\sigma_{RS}(E_{K\alpha};E_f)}{\sigma_{KX}(E_o)} \end{aligned} \tag{3.24}$$

where

$$\xi(E_o) = \frac{\varepsilon_R}{\varepsilon_X} (1 - \varepsilon_X) \frac{\sigma_{KX}(E_o)}{\sigma_{ABS}(E_{K\alpha})} \, . \tag{3.25}$$

Using $\frac{\varepsilon_R}{\varepsilon_X} \sim 1$, $\varepsilon_X \sim 0.5$, and $\sigma_{ABS}(E_{K\alpha}) = 1.615 \times 10^4 b$, we obtain $\xi(E_o = 1.0\ MeV) = 10.12 \times 10^{-3}$, $\xi(E_0 = 1.5\ MeV) = 15.76 \times 10^{-3}$, and $\xi(E_0 = 2.0\ MeV) = 19.57 \times 10^{-3}$ in reasonable agreement (dashed lines in Fig. (8)) with the detailed calculation.

Numerical Considerations:

(a) Integration Technique (See also Appendix B)

The integrals $I_R(\alpha,\beta;E_f)$ and $I_F(\alpha,\beta)$ given in Eqns. (3.13) and (3.14) respectively were evaluated using a standard Gauss-Legendre quadrature formula for an arbitrary interval:[17]

$$\int_a^b f(y)dy = \frac{b-a}{2} \sum_{i=1}^{n} \omega_i f(y_i) + R_n \tag{3.26}$$

where

$$y_i = \left(\frac{b-a}{2}\right) x_i + \left(\frac{b+a}{2}\right)$$

$$\omega_i = 2/\{(1-x_i^2)[P_n'(x_i)]^2\}$$

$$R_n = \frac{(b-a)^{2n+1}(n!)^4}{(2n+1)[(2n)!]^3}\ 2^{2n+1}\ f^{(2n)}(\chi) \tag{3.27}$$

and x_i is the i^{th} zero of $P_n(x)$. The appropriate values of x_i and ω_i are tabulated in Ref. (18). The integral $I_F(\alpha,\beta)$ was calculated using a single 12-point formula while the triple integrals in $I_R(\alpha,\beta;E_f)$ were evaluated using three nested 8-point formulas. The 8-point formulas were chosen as a convenient compromise between cost and accuracy. The

Figure 8 Relative x-ray production efficiency in the immediate vicinity of the Raman edge and appropriate for our particular experimental geometry ($\alpha = \beta = 45°$).

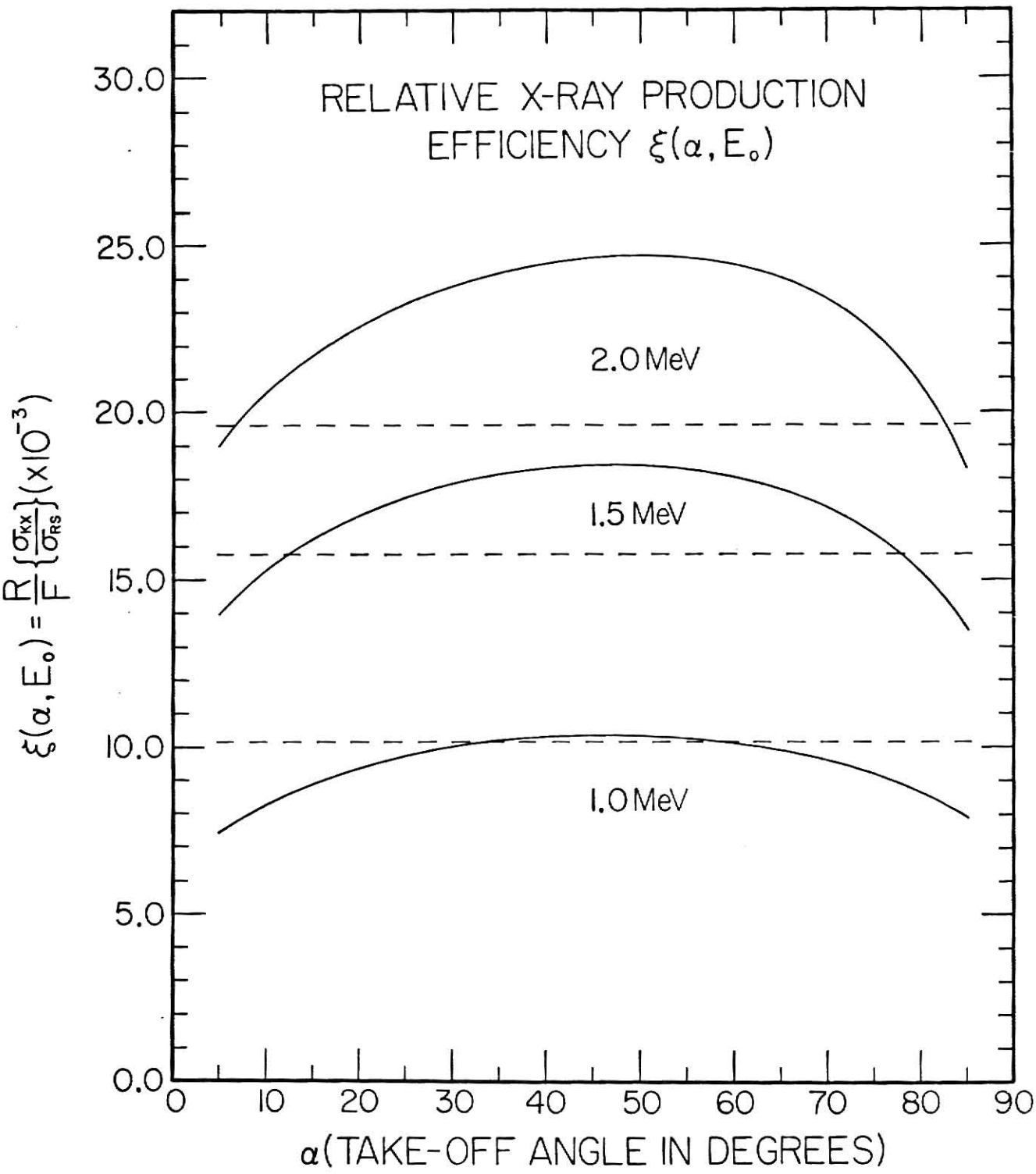
RELATIVE X-RAY PRODUCTION
EFFICIENCY $\xi(\alpha, E_o)$
2.0 MeV
1.5 MeV
1.0 MeV
$\xi(\alpha, E_o) = \frac{R}{F}\left\{\frac{\sigma_{Kx}}{\sigma_{Rs}}\right\}(\times 10^{-3})$
30.0
25.0
20.0
15.0
10.0
5.0
0.0
0
10
20
30
40
50
60
70
80
90
α(TAKE-OFF ANGLE IN DEGREES)

remainder term R_n was not actually calculated due to the high order of the functional derivative required. Instead, convergence tests using a 24-point formula for $I_F(\alpha,\beta)$ and nested (24,16,12)-point formulas for $I_R(\alpha,\beta;E_f)$ were performed. In all cases tested the resulting error in the relative x-ray production efficiency $\xi(\alpha,\beta;E_o,E_f)$ (See Table I) was found to be less than 0.4%. The infinite limit which appears in the expression for $I_R(\alpha,\beta;E_f)$ was reduced to r_{max} for computational purposes where r_{max} is such that the Raman rate within dV due to Kα radiation from dV' (Eqn. (2.7)) is attenuated by a factor of 1000. The resulting cutoff error in $\xi(\alpha,\beta;E_o,E_f)$ was found to be less than 0.02%.

(b) X-Ray Production Cross Section; $\sigma_{KX}(E(s))$

Silicon K x-ray production cross sections, $\sigma_{KX}(s)$, as a function of ion penetration depth were obtained by combining the K x-ray production cross section vs. ion energy, $\sigma_{KX}(E)$, with the corresponding ion energy vs. depth, E(s), calculations. PWBABC cross sections for protons on silicon were obtained from the program XCODE listed in Ref. (19). The calculations are based on theories which assume that the ionization is produced by direct Coulomb excitation of the target electrons by the incident projectile. These calculations assume that the projectile acts as a bare nuclear charge and thus should be reliable for incident protons. The silicon K-shell fluorescence yield used was 0.0412 as calculated by McGuire.[20] Ion energy as a function of target penetration depth was obtained by the simple iterative process outlined below:

Figure 9 H^+ + Si x-ray production cross section as a function of ion penetration depth.

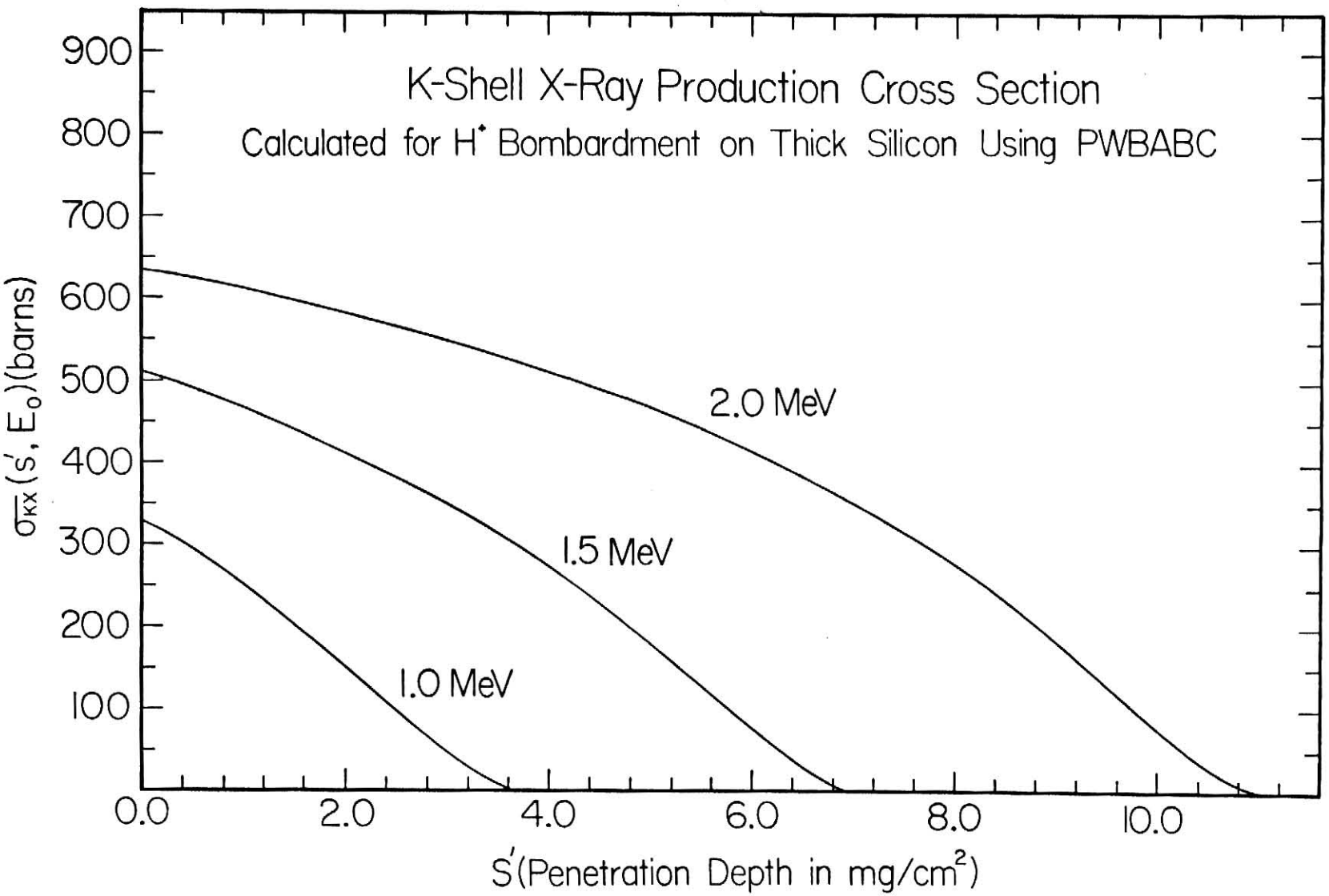
K-Shell X-Ray Production Cross Section
Calculated for H⁺ Bombardment on Thick Silicon Using PWBABC
$\sigma_{Kx}(s', E_0)$(barns)
900
800
700
600
500
400
300
200
100
2.0 MeV
1.5 MeV
1.0 MeV
0.0
2.0
4.0
6.0
8.0
10.0
S'(Penetration Depth in mg/cm²)

$$E(0) \equiv E_o$$

$$E(\Delta s) = E_o - (\Delta s)\left(\frac{dE}{ds}\right)_{E_o} \equiv E_1$$

$$E(2\Delta s) = E_1 - (\Delta s)\left(\frac{dE}{ds}\right)_{E_1} \equiv E_2$$

$$E(3\Delta s) = E_2 - (\Delta s)\left(\frac{dE}{ds}\right)_{E_2} \equiv E_3$$

where Δs is such that $(\Delta s)\left(\frac{dE}{ds}\right)_{E_i} << E_i$. In general we have:

$$E(n\Delta s) = E_{n-1} - (\Delta s)\left(\frac{dE}{ds}\right)_{E_{n-1}} \equiv E_n \quad . \tag{3.28}$$

The energy loss vs. E, $\frac{dE}{ds}(E)$, was calculated based on data given in Ref. (21). For computational purposes the calculated $\sigma_{KX}(s)$ data were fit to a fifth order polynomial in ion penetration depth, s.

(c) Mass Attenuation Coefficients; $\mu_2(E_{K\alpha})$, $\mu_3(E_f)$

The mass attenuation coefficients μ_2 and μ_3 as a function of photon wavelength are given in general by:

$$\mu = a\,\lambda^b\,Z^c \tag{3.29}$$

where Z is the nuclear charge of the medium and a, b, and c are constants over a given range of λ. Writing both μ_2 and μ_3 in this form we may obtain an expression for μ_3 in terms of known quantities:

$$\mu_3 = \mu_2 \left(\frac{\lambda_f}{\lambda_{K\alpha}}\right)^b = \mu_2 \left(\frac{E_{K\alpha}}{E_f}\right)^b \quad . \tag{3.30}$$

For λ(K edge) < λ < $\lambda(L_1$ edge) Ref. (16) gives b = 2.74. Using the values $\mu_2 = 0.346289 \frac{cm^2}{mg_2}$ (±2%), $E_{K\alpha}$ = 1739.78 eV, and E_f = 1640.58 eV we obtain $\mu_3 = 0.406724 \frac{cm}{mg}$ (±2%). Note that for E_f we have used the maximum scattered photon energy, $E_{K\alpha} - E(L_{2,3}(\text{Binding}))$. The variation in μ_3 over the approximately 6 eV visible width of the Raman edge is less than 1% of the value stated above. Thus, setting $E_f = E_f(\text{MAX})$ in the numerical calculation of $\xi(\alpha,\beta;E_o,E_f)$ in the vicinity of the edge should not be a large source of error.

DATA ANALYSIS AND CONCLUSION

(a.) Data Analysis

The motivation for doing this experiment was to investigate the internal resonance Raman scattering phenomenon in ion-induced x-ray spectra. This was accomplished by studying the K x-ray spectra of thick Si targets produced by proton impact. Fig. 10 shows the results of Si bombarded with 1.5 and 2.0 MeV proton beams. The structure between 1630 and 1640 eV is attributed to the IRRS process with the ejected electron having very nearly zero energy and the photon having approximately the Si Kα energy minus the $L_{2,3}$ ionization energy. The peak at 1650 eV has been identified[1] as the first line in the RER satellite sequence (KL^1 RER). The RER intensity is seen to decrease in going from 1.5 to 2.0 MeV since we are well beyond matched velocity for L-shell ionization ($\sim$ 0.18 MeV). The RAE edge is easily seen between 1600 and 1620 eV. Considerable structure whose origin is not fully understood is seen in this region.

In the introduction to this thesis and in Section II we established the spectral shape of the resonance Raman process to be that of an inverted absorption edge tailing off at low energies. From Fig. 10 we can see that only a small portion ($\sim$ 6 eV) of the total width of this edge structure is actually visible amid the diverse background of our spectra. Thus, unless the analytical shape and background of the Raman edge are known, it becomes impossible to directly measure the total cross section $\sigma_{RS}(E_i = E_{K\alpha})$ associated with the resonance Raman process from our data. However, it is possible to directly measure a partial scattering cross section associated with scattering into an energy

Figure 10 Low energy Si K x-ray spectra induced by proton bombardment. The spectra shown are each the sum of several independent spectra. The sum was then compressed 5 channels to 1 channel to obtain the plots shown. In each spectra there are approximately 10000 counts above background in the visible portion of the Raman edge.

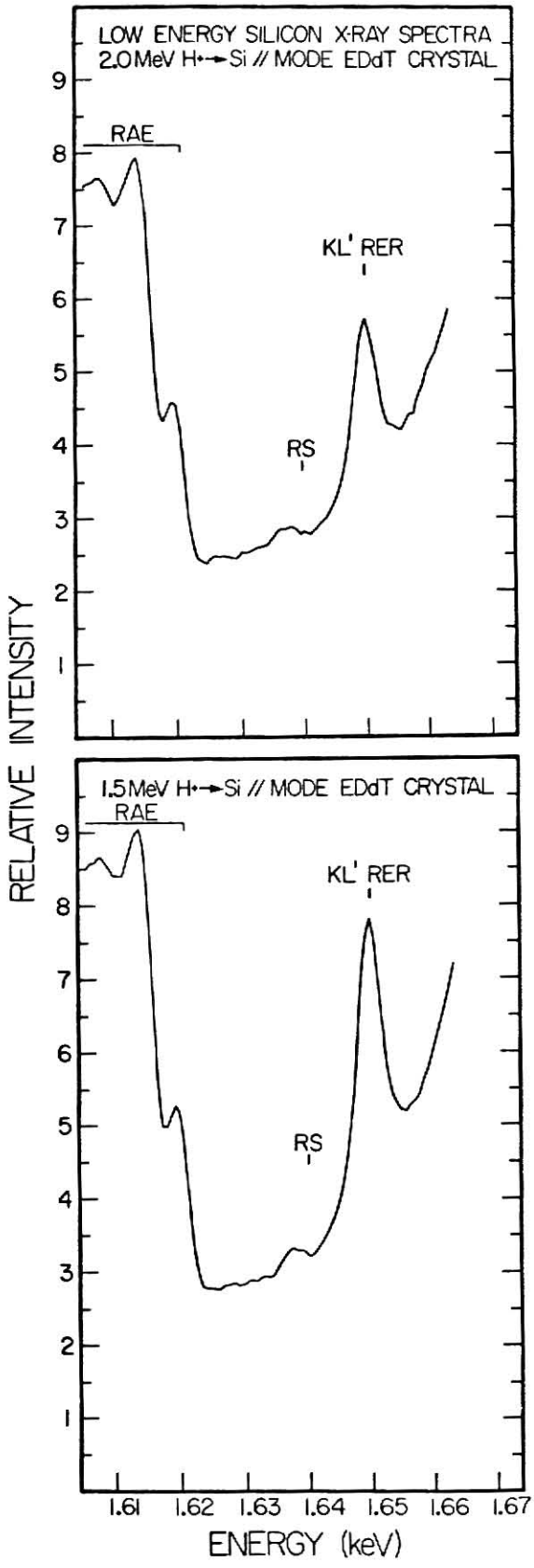
LOW ENERGY SILICON X-RAY SPECTRA
2.0 MeV H+ → Si // MODE EDdT CRYSTAL
RAE
KL' RER
RS
1.5 MeV H+ → Si // MODE EDdT CRYSTAL
RAE
KL' RER
RS
RELATIVE INTENSITY
ENERGY (keV)
1.61
1.62
1.63
1.64
1.65
1.66
1.67

interval $\sim 1634 \leq E_f \leq E_f(\max) = 1640.58$ eV and from that partial cross section to estimate the total cross section $\sigma_{RS}(E_i = E_{K\alpha})$ for scattering into all angles and all allowed energies ($0 \leq E_f \leq E_f(\max)$).

The partial scattering cross section in the immediate vicinity of the Raman edge may be calculated using the results of Section III (Eqn. (3.19)) if the relative intensity $RS/K\alpha_{1,2} = R(\alpha,\beta;E_f)/F(\alpha,\beta)$ is known. One method for determining this relative intensity is the following:

$$\frac{RS}{K\alpha_{1,2}} = \frac{RS}{KL^1RER} \times \frac{KL^1RER}{K\alpha L^1} \times \frac{K\alpha L^1}{K\alpha_{1,2}} \tag{4.1}$$

where $K\alpha L^1$ is the intensity of the first Kα satellite line. This approach has both advantages and disadvantages associated with it relative to direct measurement of $RS/K\alpha_{1,2}$. Combining three separate relative intensity measurements results in a more complicated statistical error in $RS/K\alpha_{1,2}$ and yet, on the other hand, a direct measurement involves a detailed knowledge of the properties of the spectrometer analyzing crystal (surface reflection, absorption edges, etc.) over a wide range of energies. Additionally, a direct measurement involves a careful normalization between the IRRS and characteristic radiation portions of the spectra where the beam current was much different. In view of these difficulties we have chosen to use the method of Eqn. (4.1).

The ratios RS/KL^1RER and $K\alpha L^1/K\alpha_{1,2}$ are measured in this experiment while $KL^1RER/K\alpha L^1$ has been measured previously by Jamison et al.[1] The measured values of the ratios involved are tabulated in Table II. Due to the low intensity and uncertain background in the

IRRS region the intensity of the Raman edge was taken as the integrated intensity below the edge ($\sim$ 6 eV) minus a trapezoidal background. The RER intensity was taken as the area of a Gaussian peak sitting on a background. The background was taken as a constant plus a Lorentzian tail due to the characteristic radiation. A χ^2 (best least-squares) fit was made to each of the RER peaks allowing the RER parameters and background parameters to vary simultaneously. The intensities of the Kα and first satellite (KαL^1) line were taken as the integrated intensities of each of the well resolved peaks.

Based on our most reliable data (Fig. 10) we obtain values for the relative intensity RS/K$\alpha_{1,2}$ of $1.20 \times 10^{-5} \pm 3.23 \times 10^{-6}$ at E_o(incident proton energy) = 1.5 MeV and $1.42 \times 10^{-5} \pm 4.00 \times 10^{-6}$ at E_o = 2.0 MeV. A slight rise in the relative intensity in going from 1.5 to 2.0 MeV is expected since the relative x-ray production efficiency ξ (Fig. 8) also increases slightly over this range. However, within the quoted uncertainty for RS/K$\alpha_{1,2}$ this rise is not entirely obvious. The values of $\xi(\alpha,\beta;E_o,E_f)$ in the immediate vicinity of the Raman edge (and aprpopriate for our particular experimental geometry ($\alpha = \beta = 45°$)) are tabulated in Table I. Taking ξ(1.5 MeV) = 1.8416×10^{-2}, ξ(2.0 MeV) = 2.4614×10^{-2}, σ_{KX}(1.5 MeV) = 5.09×10^{-22} cm^2, and σ_{KX}(2.0 MeV) = 6.32×10^{-22} cm^2 we may use Eqn. (3.19) to obtain $\Delta\sigma_{RS}(E_o = 1.5 \text{ MeV}) = (4.23 \pm 1.14)r_o^2$ and $\Delta\sigma_{RS}(E_o = 2.0 \text{ MeV}) = (4.65 \pm 1.31)r_o^2$ for the partial scattering cross section. The cross section appears to be independent of the incident projectile energy within experimental uncertainty as expected.

A theoretical value for the resonance contribution to the partial scattering cross section can be obtained by integrating Eqn. (2.45)

over the region of interest ($1634 \leq E_f \leq 1640.58$ eV). This yields a value of $\Delta\sigma_{RS}$(theoretical) = 3.73 r_o^2 in reasonable agreement with our experiment. The total resonant contribution to the Raman scattering cross section is obtained by integrating Eqn. (2.45) over the entire range of E_f ($0 \leq E_f \leq 1640.58$ eV). This gives σ_{RS}(theoretical) = 50.81 r_o^2. In both calculations we have used Hartree-Fock single-electron wave functions in the numerical calculation of the matrix element $\langle 1s|p_z|2p\rangle$. The 1s wave function was calculated in the presence of a 2p vacancy and the 2p wave function was calculated in the presence of a 1s vacancy. Values for the K absorption cross section $\sigma_K(\omega_{K\alpha} + \omega_i - \omega_f)$ were taken from the theoretical calculations of Scofield.[22]

The theoretical partial scattering cross section as calculated amounts to 7.34% of the total theoretical cross section. Thus it is possible to estimate the total scattering cross section from our data based on the assumption that we are able to measure approximately the same percentage of the total cross section. This gives an estimate for the total cross section of σ_{RS}(Exp.) = $(60.48 \pm 11.80)r_o^2$ where we have based our calculation on the average of $\Delta\sigma_{RS}(E_o = 1.5$ MeV) and $\Delta\sigma_{RS}(E_o = 2.0$ MeV). Note that our theoretical calculations include only the resonant contribution to the total scattering cross section whereas our experimental measurements can be expected to include both resonant and non-resonant contributions. The numerical change in the scattering cross section caused by inclusion of the non-resonant contribution is difficult to predict but is expected to be small.[11] Cross section values are tabulated in Table III.

(b.) *Conclusion and Comments*

We have presented an experimental study of the internal resonance Raman scattering process in ion induced Si K x-ray spectra obtained from thick targets. We have identified the IRRS structure in our spectra based on both its predicted spectral shape and edge energy. We were able to measure a partial scattering cross section associated with this process which was in reasonable agreement with theoretical calculations. From this partial cross section we were able to estimate a value for the total scattering cross section into all angles and all allowed energies.

We have restricted our experiment to incident proton beams in order to minimize unwanted background in the IRRS region. The use of proton beams also has the effect of minimizing the amount of L-shell ionization in the target. This increases the normal Kα yield and hence also the IRRS intensity. We have also restricted our study of the IRRS process to a single target element, Si. This was done in view of the difficulty of obtaining pure solid targets capable of withstanding high beam currents in the immediate range above Z = 14. Additionally, O. Keski-Rahkonen[23] has estimated that the cross section drops off with increasing Z although we have not investigated the Z dependence of the cross section in this work. Finally, we have not investigated the predicted dependence of the relative x-ray production efficiency ξ (shown in Fig. 8) on the experimental geometry in the case of $\alpha \neq \beta$. Based on the experimental uncertainties in our determination of $RS/K\alpha_{1,2}$ at $\alpha = \beta = 45°$ it is unlikely that any angular dependence could be justifiably observed without much better statistics.

Certainly analyzing ion induced x-ray spectra should not be thought of as an optimal (or even desirable) method for investigating the IRRS process. Photon induced spectra and, to an even greater extent, spectra induced by synchroton radiation are capable of providing both higher count rates and lower background in the IRRS region. Synchroton radiation offers the added advantage of being able to "tune" the energy of the incident radiation over a wide range of energies in order to study the energy systematics of the IRRS process. The significance of the observation of the IRRS process in ion induced x-ray spectra then seems finally to rest upon two points: (1) it establishes, as has been noted here and in other work,[4] a distinct, observable difference between scattering-type processes which are internal to the atom (RAE) and those which are external to the atom (IRRS) and, (2) it establishes the fact that inelastic photon scattering processes are observable phenomena in thick target x-ray spectra.

REFERENCES

1. K. A. Jamison, J. M. Hall, J. Oltgen, C. W. Woods, Robert L. Kauffman, Tom J. Gray, and Patrick Richard, Phys. Rev. A 14, 937 (1976).
2. T. Åberg and J. Utriainen, J. de Physique, C4, 295 (1971).
3. T. Åberg, private communication.
4. T. Åberg and J. Utriainen, Phys. Rev. Lett. 22, 1346 (1969).
5. K. A. Jamison, J. M. Hall, and Patrick Richard, J. Phys. B 8, L458 (1975).
6. M. Sawada, K. Taniguchi, and H. Nakamura, J. Phys. Soc. Japan 33, 1496 (1972).
7. C. J. Sparks, Jr., Phys. Rev. Lett. 33, 262 (1974).
8. Y. B. Bannett, J. I. Gersten, N. Tzoar, and I. Freund, Phys. Rev. Lett. 36, 882 (1976).
9. P. Eisenberger, P. M. Platzman, and H. Winick, Phys. Rev. B 13, 2377 (1976).
10. Y. B. Bannett and I. Freund, Phys. Rev. Lett. 34, 372 (1975).
11. J. Tulkki and T. Åberg, private communication.
12. B. Curnutte, J. Spangler, and L. Weaver, "Theory of Radiation and Radiative Transitions," in Methods of Experimental Physics , edited by D. Williams (Academic Press 1976) Vol. 13A, p. 31.
13. W. Heitler, The Quantum Theory of Radiation (Clarendon Press 1954) Chapter V.
14. Since the stopping of an ion in a solid is essentially a statistical process we expect there to be a statistical fluxuation about the point corresponding to the average range. Calculations for H^+ + Si in the 1.0 - 2.0 MeV range give a percent deviation in the ion range

of $\sigma_R/R \sim 0.04\%$.

15. Calculations of the differential elastic scattering cross section for H^+ + Si in the 1.0 - 2.0 MeV range using a screened Coulomb potential in the first Born approximation indicates that the scattering cross section drops off by $\sim$ 10 orders of magnitude in the first degree from the normal.

16. R. Theisen and D. Vollath, "Tables of X-Ray Mass Attenuation Coefficients," (Verlag Stahleisen M. B. H. Dusseldorf 1967).

17. B. Carnahan and J. O. Wilkes, Digital Computing and Numerical Methods (John Wiley and Sons 1973) p. 339.

18. M. Abramowitz and I. A. Stegun, Handbook of Mathematical Functions (NBS 1968) p. 916.

19. G. H. Pepper, Ph.D. Dissertation, North Texas State University, 1974.

20. W. Banbynek, B. Crasemann, R. W. Fink, H. U. Freund, H. Mark, C. D. Swift, R. E. Price, and P. V. Rao, Rev. Mod. Phys. 44, 716 (1972).

21. C. F. Williamson, J. P. Boujot, J. Picard, "Tables of Range and Stopping Power of Chemical Elements for Charged Particles and Energy 0.05 to 500 MeV," (Commissariat A L'Energie Atomique Report CEA-R 3042, 1966).

22. J. H. Scofield, "Theoretical Photoionization Cross Sections from 1 to 1500 keV," (Lawrence Livermore Laboratory UCRL-51326, 1973).

23. O. Keski-Rahkonen, private communication.

24. I. S. Gradshteyn and I. M. Ryzhik, Tables of Integrals, Series, and Products (Academic Press 1965).

25. D. A. Shirley, Phys. Rev. A 7, 1520 (1973).

26. J. A. Bearden, Rev. Mod. Phys. 39, 78 (1967).

TABLE I

RELATIVE X-RAY PRODUCTION EFFICIENCY, $\xi(\alpha, E_o)$ [a]
(Based on Eqn. (3.18))

α(Degrees)	$\xi(\alpha; E_o=1.00$ MeV) $(\times 10^3)$	$\xi(\alpha; E_o=1.50$ MeV) $(\times 10^3)$	$\xi(\alpha; E_o=2.00$ MeV) $(\times 10^3)$
5	7.450 (.005%)[b]	14.010 (.008%)[b] (0.37%)[c]	19.021 (.012%)[b]
10	8.285	15.303	20.578
15	8.890	16.214	21.701
20	9.356	16.898	22.562
25	9.716	17.424	23.224
30	9.986	17.827	23.746
35	10.177	18.123	24.143
40	10.297	18.319	24.430
45	10.348 (.009%)[b]	18.416 (.011%)[b] (0.03%)[c]	24.614 (.015%)[b]
50	10.335	18.412	24.687
55	10.257	18.298	24.636
60	10.109	18.060	24.435
65	9.888	17.676	24.043
70	9.582	17.113	23.395
75	9.177	16.318	22.390
80	8.643	15.198	20.844
85	7.916 (.012%)[b]	13.554 (.012%)[b] (0.01%)[c]	18.353 (.011%)[b]

a) In this case α and β have been experimentally constrained such that $\alpha + \beta = 90°$. Thus α is equivalent to the target take-off angle measured relative to the target surface (see Fig. (7)). The efficiency ξ has been calculated in the immediate vicinity of the Raman edge (i.e. $E_f = E_f(MAX) = 1640.58$ eV has been used).

b) Estimated cutoff error in calculation.

c) Estimated convergence error in calculation

TABLE II

EXPERIMENTAL RELATIVE INTENSITY RATIOS[a]

(E_o(MeV)/Crystal)	Relative Intensity	
(1.5/ADP)	RS/KL^1RER	= 0.0340 ± 0.011 (32%)
	$RS/K\alpha_{1,2}$	= $8.54 \times 10^{-6} \pm 3.55 \times 10^{-6}$ (42%)
(1.5/EDdT)	RS/KL^1RER	= 0.0477 ± 0.0034 (7%)
	$KL^1RER/K\alpha L^1$	= 0.0016 ± 0.0004 (25%)[b]
	$K\alpha L^1/K\alpha_{1,2}$	= 0.157 ± 0.011 (7%)
	$RS/K\alpha_{1,2}$	= $1.20 \times 10^{-5} \pm 3.23 \times 10^{-6}$ (27%)
(2.0/EDdT)	RS/KL^1RER	= 0.0684 ± 0.0056 (8%)
	$KL^1RER/K\alpha L^1$	= 0.0016 ± 0.0004 (25%)[b]
	$K\alpha L^1/K\alpha_{1,2}$	= 0.130 ± 0.013 (10%)
	$RS/K\alpha_{1,2}$	= $1.42 \times 10^{-5} \pm 4.00 \times 10^{-6}$ (28%)

a) All intensities were measured with the spectrometer in the ‖ mode.

b) Jamison et al.[1]

TABLE III

IRRS CROSS SECTIONS IN r_o^2

(E_o(MeV)/Crystal)	$\Delta\sigma_{RS}$(EXP.)[a]	σ_{RS}(EXP.)[b]
(1.5/ADP)	3.01 ± 1.25	41.0 ± 17.1
	[3.52 ± 1.46][c]	[48.0 ± 19.9]
(1.5/EDdT)	4.23 ± 1.14	57.7 ± 15.5
	[4.94 ± 1.33]	[67.3 ± 18.1]
(2.0/EDdT)	4.65 ± 1.31	63.4 ± 17.9
	[5.85 ± 1.65]	[79.7 ± 22.5]
	AVE.[d] = 4.44 ± 0.87	AVE.[d] = 60.5 ± 11.8
(THEORETICAL)[e]	3.78	50.81

a) Partial cross section for scattering into $1634 \leq E_f \leq E_f(\max) = 1640.58$.

b) Estimate of total scattering cross section based on $\Delta\sigma_{RS}$(EXP.) in the manner of Section IV.

c) Values in brackets are based on the simplified thick target analysis resulting in Eqn. (3.24).

d) Average of 1.5 and 2.0 MeV EDdT data.

e) Based on Eqn. (2.45) integrated over the appropriate range of E_f.

APPENDIX A

A useful analogy to the development of $R(\alpha,\beta;E_f)/F(\alpha,\beta)$ given in Section III is that of photon induced internal Raman scattering. A development of the photon induced case similar to that given here has been made previously by O. Keski-Rahkonon (Ref. (23)). In this case characteristic Kα photons are produced within a thick solid target as a result of K ionization produced by external photon (rather than ion) bombardment. The essential steps in the development given in Section III remain unchanged. The incident radiation will be treated as a parallel, monochromatic beam of intensity I_o, energy E_o, and arbitrary cross section. A thin layer of thickness dt' located parallel to the target surface at a depth t' is exposed to an incident photon rate given by:

$$I_o\, dA'\cos\alpha\, e^{-\mu_1 s'} = I_o\, dA'\cos\alpha\, e^{-\mu_1 t'/\cos\alpha} \qquad (A.1)$$

where $\mu_1 = \mu_1(E_o)$ is the total linear absorption coefficient for the monochromatic primary radiation. The total number of photoabsorptions per unit time within the volume element $dV' = (dA'\cos\alpha)ds' = dA'dt'$ under consideration is:

$$I_o\, dV'\mu_{PE}\, e^{-\mu_1 t'/\cos\alpha} \qquad (A.2)$$

where μ_{PE} is the photoelectric component of μ_1 responsible for producing K-shell vacancies. Thus, the rate of Kα photon production within the volume element dV' is given by:

$$I_o \, dV' \omega_{KX} \mu_{PE} \, e^{-\mu_1 t'/\cos\alpha} \tag{A.3}$$

where ω_{KX} is the K-shell fluorescence yield.

The total detectable Raman yield due to Kα radiation from dV' is:

$$R(dV';E_f) \equiv I_o \frac{dV'}{4\pi} \omega_{KX} \mu_{PE} n d\sigma_{RS} (d\Omega_\beta/4\pi) e^{-\mu_1 t'/\cos\alpha}$$

$$\times \int_V e^{-\mu_2 r - \mu_3 t/\cos\beta} \sin\theta d\theta d\phi dr \quad . \tag{A.4}$$

A factor K is defined to be

$$K \equiv I_o \frac{dV'}{2} \omega_{KX} \mu_{PE} n d\sigma_{RS} (d\Omega_\beta/4\pi)$$

and it is again noted that $t = t' - r\cos\theta$ so that upon integration over $d\phi$ Eqn. (A.4) can be written as:

$$R(dV';E_f) = K \, e^{-(\mu_1/\cos\alpha + \mu_3/\cos\beta)t'}$$

$$\times \left\{ \int_0^{t'} \int_{-1}^{1} e^{\mu_3 r\cos\theta/\cos\beta - \mu_2 r} \, d(\cos\theta) dr \right.$$

$$\left. + \int_{t'}^{\infty} \int_{-1}^{\frac{t'}{r}} e^{\mu_3 r\cos\theta/\cos\beta - \mu_2 r} \, d(\cos\theta) dr \right\} \quad . \tag{A.5}$$

The development up to here has been conceptually the same as that leading

up to Eqn. (3.8) in the ion induced case. However, in this case the exponential dependence of Kα photon production on target depth allows us to perform the required integrations analytically rather than numerically. Thus:

$$R(dV';E_f) = K\, e^{-(\mu_1/\cos\alpha + \mu_3/\cos\beta)t'} \times \left(\frac{\cos\beta}{\mu_3}\right)(2I_1 + I_2 e^{\mu_3 t'/\cos\beta} - I_3) \qquad (A.6)$$

where

$$I_1 \equiv \int_0^{t'} \frac{e^{-\mu_2 r}}{r} \sinh(\mu_3 r/\cos\beta)\,dr$$

$$I_2 \equiv \int_{t'}^{\infty} \frac{e^{-\mu_2 r}}{r}\,dr$$

$$I_3 \equiv \int_{t'}^{\infty} \frac{e^{-\mu_3 r/\cos\beta - \mu_2 r}}{r}\,dr \quad . \qquad (A.7)$$

Eqn. (A.6) can be integrated over s' = (0,∞) to obtain the total detectable Raman yield (E_f component) due to Kα radiation from a column of differential cross section dA'cosα along the beam path. With the definitions

$$\lambda \equiv \mu_1/\cos\alpha + \mu_3/\cos\beta$$

$$\gamma \equiv \mu_3/\cos\beta + \mu_2$$

we have:

$$R(\alpha,\beta;E_f) = I_o \frac{dA'}{2} \cos\alpha\, \omega_{KX}\mu_{PE}^{n}d\sigma_{RS}(d\Omega_\beta/4\pi)\frac{\cos\beta}{\mu_3}$$

$$\times \int_o^\infty e^{-\lambda t'} (2I_1 + I_2 e^{\mu_3 t'/\cos\beta} - I_3)ds'$$

$$= I_o \frac{dA'}{2} \omega_{KX}\mu_{PE}^{n}d\sigma_{RS}(d\Omega_\beta/4\pi)\frac{\cos\beta}{\mu_3}$$

$$\times \int_o^\infty e^{-\lambda t'} (2I_1 + I_2 e^{\mu_3 t'/\cos\beta} - I_3)dt'$$

$$= I_o \frac{dA'}{2} \omega_{KX}\mu_{PE}^{n}d\sigma_{RS}(d\Omega_\beta/4\pi)\frac{\cos\beta}{\mu_3} (2I_4+I_5-I_6) \quad (A.8)$$

where

$$I_4 \equiv \int_o^\infty e^{-\lambda t'} \int_o^{t'} \frac{e}{r}^{-\mu_2 r} \sinh(\mu_3 r/\cos\beta)dr\, dt'$$

$$I_5 \equiv \int_o^\infty e^{-\mu_1 t'/\cos\alpha} \int_{t'}^\infty \frac{e}{r}^{-\mu_2 r} dr\, dt'$$

$$I_6 \equiv \int_o^\infty e^{-\lambda t'} \int_{t'}^\infty \frac{e}{r}^{-\gamma r} dr\, dt' \quad . \quad (A.9)$$

Interchanging the order of integration and referring to Ref. (24), we obtain:

$$I_4 = \frac{1}{2\lambda} \ln\left\{\frac{\mu_2 + \mu_1/\cos\alpha + 2\mu_3/\cos\beta}{\mu_2 + \mu_1/\cos\alpha}\right\}$$

$$I_5 = \frac{\cos\alpha}{\mu_1} \ln\left\{\frac{\mu_2 + \mu_1/\cos\alpha}{\mu_2}\right\}$$

$$I_6 = \frac{1}{\lambda} \ln\left\{\frac{\mu_2 + \mu_1/\cos\alpha + 2\mu_3/\cos\beta}{\mu_2 + \mu_3/\cos\beta}\right\} \quad . \quad (A.10)$$

Thus we have:

$$R(\alpha,\beta;E_f) = I_o \frac{dA'}{2} \omega_{KX}\mu_{PE} n d\sigma_{RS}(d\Omega_\beta/4\pi)\frac{\cos\beta}{\mu_3}$$

$$\times\left[\frac{1}{\lambda}\ln\left\{\frac{\mu_2 + \mu_3/\cos\beta}{\mu_2 + \mu_1/\cos\alpha}\right\} + \frac{\cos\alpha}{\mu_1}\ln\left\{\frac{\mu_2 + \mu_1/\cos\alpha}{\mu_2}\right\}\right] . \quad (A.11)$$

The detectable Kα photon yield from the volume element dV' is given by:

$$I_o\, dV'\, \omega_{KX}\mu_{PE}(d\Omega_\beta/4\pi)\, e^{-(\mu_1/\cos\alpha + \mu_2/\cos\beta)t'} . \quad (A.12)$$

The total detectable Kα yield from the differential column discussed above is found by integrating Eqn. (A.12) along the beam path:

$$F(\alpha,\beta) \equiv I_o\, dA'\cos\alpha\, \omega_{KX}\mu_{PE}(d\Omega_\beta/4\pi) \int_o^\infty e^{-(\mu_1/\cos\alpha + \mu_2/\cos\beta)t'} ds'$$

$$= I_o\, dA'\, \omega_{KX}\mu_{PE}(d\Omega_\beta/4\pi) \int_o^\infty e^{-(\mu_1/\cos\alpha + \mu_2/\cos\beta)t'} dt'$$

$$= I_o\, dA'\, \omega_{KX}\mu_{PE}(d\Omega_\beta/4\pi) \Big/ (\mu_1/\cos\alpha + \mu_2/\cos\beta) . \quad (A.13)$$

The ratio of $R(\alpha,\beta;E_f)$ to $F(\alpha,\beta)$ is now given by:

$$\frac{R(\alpha,\beta;E_f)}{F(\alpha,\beta)} = \frac{nd\sigma_{RS}}{\mu_3}\frac{\cos\beta}{2}(\mu_1/\cos\alpha + \mu_2/\cos\beta)$$

$$\times\left[\left\{\frac{1}{\mu_1/\cos\alpha + \mu_3/\cos\beta}\right\} \ln\left\{\frac{\mu_2 + \mu_3/\cos\beta}{\mu_2 + \mu_1/\cos\alpha}\right\}\right.$$

$$\left. + \frac{\cos\alpha}{\mu_1}\ln\left\{\frac{\mu_2 + \mu_1/\cos\alpha}{\mu_2}\right\}\right]. \qquad (A.14)$$

Changing all linear absorption coefficients (cm^{-1}) to mass absorption coefficients (cm^2/mg) introduces a factor of $1/\rho$ into Eqn. (A.14). Thus we obtain:

$$\frac{R(\alpha,\beta;E_f)}{F(\alpha,\beta)} \rightarrow \frac{1}{\rho}\frac{R(\alpha,\beta;E_f)}{F(\alpha,\beta)}$$

$$= d\sigma_{RS}(E_{K\alpha};E_f)\frac{N_A\cos\beta}{2A_m\mu_3}(\mu_1/\cos\alpha + \mu_2/\cos\beta)$$

$$\times\left[\left\{\frac{1}{\mu_1/\cos\alpha + \mu_2/\cos\beta}\right\} \ln\left\{\frac{\mu_2 + \mu_3/\cos\beta}{\mu_2 + \mu_1/\cos\alpha}\right\}\right.$$

$$\left. + \frac{\cos\alpha}{\mu_1}\ln\left\{\frac{\mu_2 + \mu_1/\cos\alpha}{\mu_2}\right\}\right]. \qquad (A.15)$$

Given μ_1, μ_2, and μ_3, Eqn. (A.15) may be used to experimentally determine $\sigma_{RS}(E_i = E_{K\alpha})$ under the same conditions outlined in Section III.

APPENDIX B

This appendix consists of a listing of the two computer codes used to evaluate the integrals $I_R(\alpha,\beta;E_f)$ and $I_F(\alpha,\beta)$ of Section III.

ILLEGIBLE DOCUMENT

THE FOLLOWING DOCUMENT(S) IS OF POOR LEGIBILITY IN THE ORIGINAL

THIS IS THE BEST COPY AVAILABLE

MAIN PROGRAM FOR CALCULATING RAMAN SCATTERING INTEGRAL

```
      IMPLICIT REAL*8(A-H,O-Z)
      DIMENSION X1(30), W1(30), Y1(30), WF1(30)
      DIMENSION X2(30), W2(30), Y2(30), WF2(30)
      DIMENSION X3(30), W3(30), Y3(30), WF3(30)
C
C****   DATA AQUISITION AND OUTPUT OF INITIAL DATA
C
      READ(5,5) N1
      N1HALF=N1/2
      READ(5,8) (X1(N1-J+1),W1(N1-J+1), J=1,N1HALF)
      DO 25 J=1,N1HALF
      X1(J)=-X1(N1-J+1)
      W1(J)=W1(N1-J+1)
25    CONTINUE
      READ(5,5) N2
      N2HALF=N2/2
      READ(5,8) (X2(N2-J+1),W2(N2-J+1), J=1,N2HALF)
      DO 26 J=1,N2HALF
      X2(J)=-X2(N2-J+1)
      W2(J)=W2(N2-J+1)
26    CONTINUE
      READ(5,5) N3
      N3HALF=N3/2
      READ(5,8) (X3(N3-J+1),W3(N3-J+1), J=1,N3HALF)
      DO 27 J=1,N3HALF
      X3(J)=-X3(N3-J+1)
      W3(J)=W3(N3-J+1)
27    CONTINUE
      READ(5,28) C0, C1, C2, C3, C4, C5
      READ(5,29) RANGE, RMAX, E0
      READ(5,10) AC2, AC3
      WRITE(6,20) N1, N2, N3
      WRITE(6,21) AC2, AC3
      WRITE(6,22) RANGE, RMAX
      WRITE(6,31) E0
      WRITE(6,23)
C
C**********   INTEGRATION ROUTINE   **********
C
30    READ(5,11) ALPH, BET, NSTOP
      ALPHA=0.017453*ALPH
      BETA=0.017453*BET
      DCALPH=DCOS(ALPHA)
      DCBETA=DCOS(BETA)
      UL3=RANGE*DCALPH
      SUM3=0.0
      DO 300 I=1,N3
      DSUM21=0.0
      Y3LAST=0.0
      Y3(I)=(UL3/2.)*X3(I)+(UL3/2.)
```

```
      GM3=AC3*Y3(I)/DCBETA
      DPT=Y3(I)/DCALPH
      CROSS=C0+(C1+(C2+(C3+(C4+C5*DPT)*DPT)*DPT)
     1*DPT)*DPT
      DO 310 JJ=1,I
      SUM21=0.0
      DO 210 J=1,N2
      Y2(J)=((Y3(JJ)-Y3LAST)/2.)*X2(J)+((Y3(JJ)
     1+Y3LAST)/2.)
      GM2=AC2*Y2(J)
      SUM11=0.0
      DO 110 K=1,N1
      GM1=AC3*Y2(J)*X1(K)/DCBETA
      GAMMA=GM3-GM1+GM2
      DEGAMM=0.0
      IF(GAMMA .LE. 37.0) DEGAMM=DEXP(-GAMMA)
C
C**************    INTEGRAND    ********************
C                                                     *
      FUNCT=CROSS*DEGAMM
C                                                     *
C*****************************************************
C
      WF1(K)=W1(K)*FUNCT
      SUM11=SUM11+WF1(K)
110   CONTINUE
      WF2(J)=W2(J)*SUM11
      SUM21=SUM21+WF2(J)
210   CONTINUE
      FSUM21=FSUM21+((Y3(JJ)-Y3LAST)/2.)*SUM21
      Y3LAST=Y3(JJ)
310   CONTINUE
      FSUM22=0.0
      BASE=Y3(I)
      JJ=2*N3-I
C***  RMAX SHOULD BE .GE. UL3
      DEC=(RMAX-BASE)/DFLOAT(JJ)
      DO 315 LL=1,JJ
      ULIM=DEC+BASE
      SUM22=0.0
      DO 220 J=1,N2
      Y2(J)=((ULIM-BASE)/2.)*X2(J)+((ULIM+BASE)/2.)
      GM2=AC2*Y2(J)
      UL12=Y3(I)/Y2(J)
      SUM12=0.0
      DO 120 K=1,N1
      Y1(K)=((UL12+1.0)/2.)*X1(K)+((UL12-1.0)/2.)
      GM1=AC3*Y2(J)*Y1(K)/DCBETA
      GAMMA=GM3-GM1+GM2
      DEGAMM=0.0
      IF(GAMMA .LE. 37.0) DEGAMM=DEXP(-GAMMA)
C
C**************    INTEGRAND    ********************
C                                                     *
```

```
      FUNCT=CROSS*DEGAMM
C                                                                      *
C**********************************************************************
C
      WF1(K)=W1(K)*FUNCT
      SUM12=SUM12+WF1(K)
120   CONTINUE
      FSUM12=((UL12+1.)/2.)*SUM12
      WF2(J)=W2(J)*FSUM12
      SUM22=SUM22+WF2(J)
220   CONTINUE
      FSUM22=FSUM22+((ULIM-BASE)/2.)*SUM22
      BASE=ULIM
315   CONTINUE
      FSUMT=FSUM21+FSUM22
      WF3(I)=W3(I)*FSUMT
      SUM3=SUM3+WF3(I)
300   CONTINUE
      FSUM3=(UL3/2.)*SUM3
C
C******    OUTPUT OF INTEGRATION VALUES    *********
C
      WRITE(6,24) ALPH, BET, FSUM3
      IF(NSTOP .EQ. 0) GO TO 30
      WRITE(6,900)
5     FORMAT(I5)
8     FORMAT(4D20.14)
10    FORMAT(2D12.7)
11    FORMAT(2D11.6,I5)
20    FORMAT(/'1N1 = ',I3/' N2 = ',I3/' N3 = ',I3///)
21    FORMAT(/' MAC2 = ',G14.7/' MAC3 = ',G14.7)
22    FORMAT(/' RANGE = ',G13.6/' RMAX = ',G14.7)
23    FORMAT(' ALPHA ',10X,'BETA ',12X,'INTEGRAL '//)
24    FORMAT(2(F6.2,9X),D14.5)
28    FORMAT(6F12.5)
29    FORMAT(2D12.7,F5.2)
31    FORMAT(/' PARAMETERS APPROPRIATE FOR INCIDENT
     1 ENERGY = ',F5.2,'MEV'///)
900   FORMAT('1END OUTPUT OF DATA '///)
      RETURN
      END
```

DATA INPUT FOR RAMAN SCATTERING PROGRAM

	COLUMN	ENTRY AND FORMAT
CARD 1 ---		
	/1-5/	NO. OF MESH POINTS FOR R INTEGRALS (8 IN THIS CASE) (I5)
CARD 2 ---		
	/1-20/	FOURTH POSITIVE ZERO OF LEGENDRE POLYNOMIAL (P8 IN THIS CASE) (D20.14)
	/21-40/	WEIGHTING FACTOR FOR FOURTH POINT (D20.14)
	/41-60/	THIRD POSITIVE ZERO (D20.14)
	/61-80/	WEIGHTING FACTOR FOR THIRD POINT (D20.14)
CARD 3 ---		
	/1-20/	SECOND POSITIVE ZERO (D20.14)
	/21-40/	WEIGHTING FACTOR FOR SECOND POINT (D20.14)
	/41-60/	FIRST POSITIVE ZERO (D20.14)
	/61-80/	WEIGHTING FACTOR FOR FIRST POINT (D20.14)

(NOTE --- NEGATIVE ZEROS ARE GENERATED BY MAIN PROGRAM. ZEROS AND WEIGHTING FACTORS MAY BE OBTAINED FROM ABRAMOWITZ AND STEGUN, PAGE 916)

CARD 4 ---		
	/1-5/	NO. OF MESH POINTS FOR COS(THETA) INTEGRALS (8 IN THIS CASE) (I5)

CARD 5 --- (SAME AS CARD 2)

CARD 6 --- (SAME AS CARD 3)

CARD 7 ---		
	/1-5/	NO. OF MESH POINTS FOR T' INTEGRAL (8 IN THIS CASE) (I5)

CARD 8 --- (SAME AS CARD 2)

CARD 9 --- (SAME AS CARD 3)

CARD 10 -- K X-RAY PRODUCTION CROSS SECTION FIT PARAMETERS

	/1-12/	C0 (F12.5)
	/13-24/	C1 "
	/25-36/	C2 "

	COLUMN	ENTRY AND FORMAT
	/37-48/	C3 (F12.5)
	/49-60/	C4 "
	/61-72/	C5 "

CARD 11 --

/1-12/	RANGE IN MG/CM**2 (D12.7)
/13-24/	MAXIMUM ALLOWED VALUE OF R IN MG/CM**2 (D12.7)
/25-29/	INCIDENT ION ENERGY IN MEV (F5.2)

CARD 12 --

/1-12/	MASS ABSORPTION COEFF. AT K ALPHA ENERGY (D12.7)
/13-24/	MASS ABSORPTION COEFF. AT RAMAN SCATTERED ENERGY (D12.7)

CARD 13 --

/1-11/	ANGLE ALPHA IN DEGREES (D11.6)
/12-22/	ANGLE BETA IN DEGREES (D11.6)
/23-27/	LEAVE BLANK IF ADDITIONAL (ALPHA, BETA) CARDS ARE TO BE ENTERED. ENTER 1 TO INDICATE LAST (ALPHA, BETA) CARD.

MAIN PROGRAM FOR CALCULATING THICK TARGET INTEGRAL

```
      IMPLICIT REAL*8(A-H,O-Z)
      DIMENSION X3(30), W3(30), Y3(30), WF3(30)
C
C*****   DATA AQUISITION AND OUTPUT OF INITIAL DATA
C
      READ(5,5) N3
      N3HALF=N3/2
      READ(5,8) (X3(N3-J+1),W3(N3-J+1), J=1,N3HALF)
      DO 27 J=1,N3HALF
      X3(J)=-X3(N3-J+1)
      W3(J)=W3(N3-J+1)
27    CONTINUE
      READ(5,28) C0, C1, C2, C3, C4, C5
      READ(5,29) RANGE, E0
      READ(5,10) AC2
      WRITE(6,20) N3
      WRITE(6,21) AC2
      WRITE(6,22) RANGE
      WRITE(6,31) E0
      WRITE(6,23)
C
C**********    INTEGRATION ROUTINE    ***************
C
30    READ(5,11) ALPH, BET, NSTOP
      ALPHA=0.017453*ALPH
      BETA=0.017453*BET
      DCALPH=DCOS(ALPHA)
      DCBETA=DCOS(BETA)
      UL3=RANGE*DCALPH
      DO 305 I=1,N3
      Y3(I)=(UL3/2.)*X3(I)+(UL3/2.)
305   CONTINUE
      SUM3=0.0
      DO 300 I=1,N3
      DPT=Y3(I)/DCALPH
      CROSS=C0+(C1+(C2+(C3+(C4+C5*DPT)*DPT)*DPT)
     1*DPT)*DPT
      GAMMA=AC2*Y3(I)/DCBETA
      DEGAMM=0.0
      IF(GAMMA .LE. 37.0) DEGAMM=DEXP(-GAMMA)
C
C*************    INTEGRAND    ******************
C                                                 *
      FUNCT=CROSS*DEGAMM
C                                                 *
C*************************************************
C
      WF3(I)=W3(I)*FUNCT
      SUM3=SUM3+WF3(I)
300   CONTINUE
```

```
      FSUM3=(UL3/2.)*SUM3
C
C*******    OUTPUT OF INTEGRATION VALUES    *********
C
      WRITE(6,24) ALPH, BET, FSUM3
      IF(NSTOP .EQ. 0) GO TO 30
      WRITE(6,900)
5     FORMAT(I5)
8     FORMAT(4D20.14)
10    FORMAT(D12.7)
11    FORMAT(2D11.6,I5)
20    FORMAT(/'1N = ',I3///)
21    FORMAT(/' MAC2 = ',G14.7)
22    FORMAT(/' RANGE = ',G13.6)
23    FORMAT(' ALPHA ',10X,'BETA ',12X,'INTEGRAL '//)
24    FORMAT(2(F6.2,9X),D14.5)
28    FORMAT(6F12.5)
29    FORMAT(D12.7,F5.2)
31    FORMAT(/' PARAMETERS APPROPRIATE FOR INCIDENT
     1 ENERGY = ',F5.2,'MEV'///)
900   FORMAT('1END OUTPUT OF DATA '///)
      RETURN
      END
```

DATA INPUT FOR THICK TARGET PROGRAM

	COLUMN	ENTRY AND FORMAT
CARD 1 ---		
	/1-5/	NO. OF MESH POINTS FOR T' INTEGRAL (12 IN THIS CASE) (I5)
CARD 2 ---		
	/1-20/	SIXTH POSITIVE ZERO OF LEGENDRE POLYNOMIAL (P12 IN THIS CASE) (D20.14)
	/21-40/	WEIGHTING FACTOR FOR SIXTH POINT (D20.14)
	/41-60/	FIFTH POSITIVE ZERO (D20.14)
	/61-80/	WEIGHTING FACTOR FOR FIFTH POINT (D20.14)
CARD 3 ---		
	/1-20/	FOURTH POSITIVE ZERO (D20.14)
	/21-40/	WEIGHTING FACTOR FOR FOURTH POINT (D20.14)
	/41-60/	THIRD POSITIVE ZERO (D20.14)
	/61-80/	WEIGHTING FACTOR FOR THIRD POINT (D20.14)
CARD 4 ---		
	/1-20/	SECOND POSITIVE ZERO (D20.14)
	/21-40/	WEIGHTING FACTOR FOR SECOND POINT (D20.14)
	/41-60/	FIRST POSITIVE ZERO (D20.14)
	/61-80/	WEIGHTING FACTOR FOR FIRST POINT (D20.14)

(NOTE --- NEGATIVE ZEROS ARE GENERATED BY MAIN PROGRAM. ZEROS AND WEIGHTING FACTORS MAY BE OBTAINED FROM ABRAMOWITZ AND STEGUN, PAGE 916)

CARD 5 --- K X-RAY PRODUCTION CROSS SECTION FIT PARAMETERS		
	/1-12/	C0 (F12.5)
	/13-24/	C1 "
	/25-36/	C2 "
	/37-48/	C3 "
	/49-60/	C4 "
	/61-72/	C5 "
CARD 6 ---		
	/1-12/	RANGE IN MG/CM**2 (D12.7)
	/13-17/	INCIDENT ION ENERGY IN MEV (F5.2)

	COLUMN	ENTRY AND FORMAT
CARD 7 ---		
	/1-12/	MASS ABSORPTION COEFF. AT K ALPHA ENERGY (D12.7)
CARD 8 ---		
	/1-11/	ANGLE ALPHA IN DEGREES (D11.6)
	/12-22/	ANGLE BETA IN DEGREES (D11.6)
	/23-27/	LEAVE BLANK IF ADDITIONAL (ALPHA, BETA) CARDS ARE TO BE ENTERED. ENTER 1 TO INDICATE LAST (ALPHA, BETA) CARD.

INTERNAL RESONANCE RAMAN SCATTERING OF CHARACTERISTIC TARGET K X RAYS IN THICK SILICON TARGETS

by

JAMES M. HALL

B.S., Southern Colorado State College, 1974

An Abstract of a Master's Thesis

submitted in partial fulfillment of the

MASTER OF SCIENCE

Department of Physics

KANSAS STATE UNIVERSITY
Manhattan, Kansas

1977

ABSTRACT

A four-inch curved crystal spectrometer has been used to investigate the internal resonance Raman scattering process in Si K x-ray spectra induced by proton bombardment of thick targets. The IRRS process involves the scattering of characteristic target Kα radiation off of the K-shell of a neighboring target atom. The scattered photons exhibit an edge shaped continuum at ∿ 1640 eV in Si which tails off at low energies. A thick target analysis is used to obtain a partial scattering cross section for scattering into an energy range ∿ $1634 \leq E_f \leq E_f(MAX) = 1640.58$ eV which is in reasonable agreement with theoretical calculations based on Fermi's Golden Rule. Based on the partial cross section we are able to estimate the total scattering cross section for scattering into all angles and all allowed energies ($0 \leq E_f \leq E_f(MAX)$).